



## LiDAR-based quantification of lava flow susceptibility in the City of Auckland (New Zealand)

Gábor Kereszturi<sup>a,\*</sup>, Jonathan Procter<sup>a</sup>, Shane J. Cronin<sup>a</sup>, Károly Németh<sup>a</sup>, Mark Bebbington<sup>a,b</sup>, Jan Lindsay<sup>c</sup>

<sup>a</sup> Volcanic Risk Solutions, Institute of Natural Resources, Massey University, Private Bag 11 222, Palmerston North, New Zealand

<sup>b</sup> Institute of Fundamental Sciences—Statistics, Massey University, Palmerston North, New Zealand

<sup>c</sup> School of Environment, The University of Auckland, PB92019, Auckland Mail Center 1142, Auckland, New Zealand

### ARTICLE INFO

#### Article history:

Received 8 December 2011

Received in revised form 16 July 2012

Accepted 20 July 2012

Available online xxxx

#### Keywords:

Digital elevation model (DEM)

Adaptive topographic classification

Drainage system

Slope angle

Volcanic hazard

Morphometric parameters

Scoria cone

Maar

Tuff ring

Monogenetic

### ABSTRACT

Lava flows represent one of the most significant volcanic hazards from basaltic monogenetic volcanoes, such as spatter cones, scoria cones, maars, and tuff rings. They are common features emanating from parasitic vents on the flanks of polygenetic volcanoes and in dominantly ‘flat-lying’ intraplate volcanic fields. The Auckland Volcanic Field (AVF) is a volcanic field that has been active for the last ca. 250 ka, hosting at least 50 monogenetic volcanoes. Morphometric parameters of lava flows, such as volume, length, thickness and area, were used to quantify the potential lava-flow inundation susceptibility to New Zealand's most densely populated area, the City of Auckland based on an airborne Light Detection and Ranging (LiDAR) Digital Surface Model (DSM). The morphometric parameters of fifteen studied flows included: average length of 2.5 km (range 0.7–6.5 km), overall average thickness of 14.8 m (range 3.4–43.8 m), average of maximum thicknesses of 48.2 m (range 18.3–180.5 m), average area occupied of 5.1 km<sup>2</sup> (range 0.4–25.1 km<sup>2</sup>) and average volume of 0.12 km<sup>3</sup> (range 0.005–1 km<sup>3</sup>). Based on these parameters and a LiDAR-derived DSM, the present topography was classified into: sea, topographic depressions; low-lying areas prone to inundation by an average lava flow; buffer zones prone to inundation only by extremely thick lava flows; and peaks or ridges, which are unlikely to be overtopped. In monogenetic fields, each new vent occurs in a new location, creating uncertainty around the spatial location of the volcanic hazard. Thus, this research provides a general vent location-independent approach to describe the lava flow susceptibility for a potentially active monogenetic volcanic field. What this analysis reveals is that the City of Auckland can be divided into two distinct areas with strongly different susceptibility to lava flow inundation. The southern part of the City is predominantly flat, without hindrance to lava flow, whereas the hilly northern and central part has many ridges that can limit or channelise lavas. These contrasting properties must be accounted for in scenario-based or probabilistic hazard and risk models developed for the AVF.

© 2012 Elsevier Inc. All rights reserved.

### 1. Introduction

Basaltic, monogenetic volcanoes often produce lava flows with a wide range in length and size (Felpeto et al., 2001; Harris & Rowland, 2001; Tucker & Scott, 2009). The length of lava flows is mostly dependent on the rate of effusion (Harris et al., 2007; Walker, 1973), the total volume (Stasiuk & Jaupart, 1997), the crystallinity and viscosity (Dragoni & Tallarico, 1994; Griffiths, 2000), the slope angle of the substratum (Favalli et al., 2009b) and other topographic features, such as valleys (Rodriguez-Gonzalez et al., 2011). To quantify and express such controlling conditions on lava flow emplacement, which are the basic inputs required of lava flow simulation codes, remotely sensed data are commonly used. For detection of active lava flows, the thermal

bands of various satellites, such as MODerate resolution Imaging Spectroradiometer (MODIS), Advanced Spaceborne Thermal Emission and Reflection radiometer (ASTER) and LANDSAT Thematic Mapper are used (Ganci et al., 2012; Harris et al., 1998; Lombardo & Buongiorno, 2006; Pieri & Abrams, 2005; Wright et al., 2004). These remote sensing data can provide information about the time-averaged discharge rates of a lava flow, which is one of the major requirements of lava flow simulations.

Lava flows related to monogenetic eruptions are commonly small in volume ( $\leq 1$  km<sup>3</sup>) and affect small areas (a few square kilometers). This small size requires at least medium (10–50 m) to high resolution ( $\leq 10$  m) imagery to map them accurately. Many types of topographic data can be used to calculate lava flow volumes including Light Detection and Ranging (LiDAR) (Harris et al., 2010), Interferometric Synthetic Aperture Radar (INSAR) (Mouginis-Mark & Garbeil, 2005), ASTER stereo image-based Digital Surface Models, i.e. DSMs (Hirano

\* Corresponding author. Tel.: +64 021 1652515.

E-mail address: [kereszturi\\_g@yahoo.com](mailto:kereszturi_g@yahoo.com) (G. Kereszturi).

et al., 2003) and Shuttle Radar Topography Mission (SRTM) (Kervyn et al., 2008) or contour-based Digital Elevation Models, i.e. DEMs (Kereszturi & Németh, 2012). These volumes could also be converted into time-averaged discharge rates (Favalli et al., 2010; Harris & Baloga, 2009; Harris et al., 2010), but the exact duration of the volcanic activity is required. In the case of monogenetic volcanic fields, where volcanic eruptions are less frequent than at polygenetic volcanoes, there is no information about the exact duration of past eruptions, posing some problems for the use of time-averaged discharge rates as a calibrator of lava flow simulations.

Apart from the lava flow parameterisation, the topography (represented digitally in a DSM or DEM) plays an important role in the emplacement of lava flows (Favalli et al., 2009b). The topography may modify the flow emplacement mechanism and channelise lava flows if the eruptive vent is located in a highly dissected topography, such as the flank of a polygenetic volcano (Mazzarini et al., 2005). The techniques to quantify and simulate lava flow behaviour described above used various algorithms to model the hazard related to lava flows from thermorheological- to topographic-dominated models. The thermorheological-dependent models require many input parameters including density, heat-preservation and composition (Crisci et al., 2004; Del Negro et al., 2008; Harris & Rowland, 2001; Hidaka et al., 2005; Vicari et al., 2007). More topography-centered codes, such as DOWNFLOW and LAZSLO are based on the probabilistic methods to establish lava flow pathways over a DSM or a DEM (Bonne et al., 2008; Connor et al., 2012; Favalli et al., 2005; Felpeto et al., 2001; Tarquini & Favalli, 2011).

Typically, lava flow simulations are performed for locations with a known vent on the flanks of a large, polygenetic volcano, e.g. Etna in Italy, or Kilauea in Hawaii (Favalli et al., 2009c; Harris & Rowland, 2001; Herault et al., 2009). On the flanks of a polygenetic volcano, the likelihood of vent-formation is significantly higher along extensional rift zones (Favalli et al., 2009c) making volcanic eruption forecasting in particular location more accurate than in many monogenetic volcanic

fields. The volcanism in Auckland in New Zealand differs from large, polygenetic volcanoes because (i) future eruptions will likely take place within a densely populated city, (ii) there are no rift zones that indicate areas of elevated hazard, and the future vent area is therefore unknown, and (iii) due to the generally low-lying topography, there are few opportunities to use mitigation options, such as artificial dams (Barberi et al., 1993; Scifoni et al., 2010). The Auckland Volcanic Field (AVF) consists of at least 50 monogenetic maars, tuff rings and scoria cones that erupted over the last 250 ka (Bebbington & Cronin, 2011; Molloy et al., 2009). The entire field (~360 km<sup>2</sup>) is located within the area of the City of Auckland, with a total population of ~1.4 million (Fig. 1). Hence, future vent forming eruptions will very likely occur within the city limits or its outskirts, allowing few mitigation or preparation options. The majority of previous scoria cones and lava flows are located in the heart of the city, upon a presently slightly elevated ridge-system (Fig. 1).

Previous studies have mostly focused on determining the location, nature and the possible effect of the future eruptions on the city (Bebbington & Cronin, 2011; Edbrooke et al., 2003; Lindsay et al., 2010; Magill & Blong, 2005a). Detailed evaluation of lava flow hazards and delimitation of potentially safe places from lava flow inundation have not yet been attempted, in spite of the relatively high level of their potential risk (Magill & Blong, 2005b). Due the high uncertainty in the location of a new vent in Auckland, the simulation of lava flow pathways is not appropriate for monogenetic field hazard analysis. In the present investigation, a vent-location independent lava flow susceptibility mapping technique is presented. This method requires only two types of information: (1) morphometry of past lava flows, such as area, volume and length characteristics, and (2) digital representation of the underlying terrain (i.e. DSM or DEM). In the present study, a resampled airborne-based LiDAR DSM was used to calculate morphometric parameters of lava flows and delimit those areas which are in relatively safe positions from lava flows using adaptive topographic classification. Based on this vent-location-independent input data, a generalised

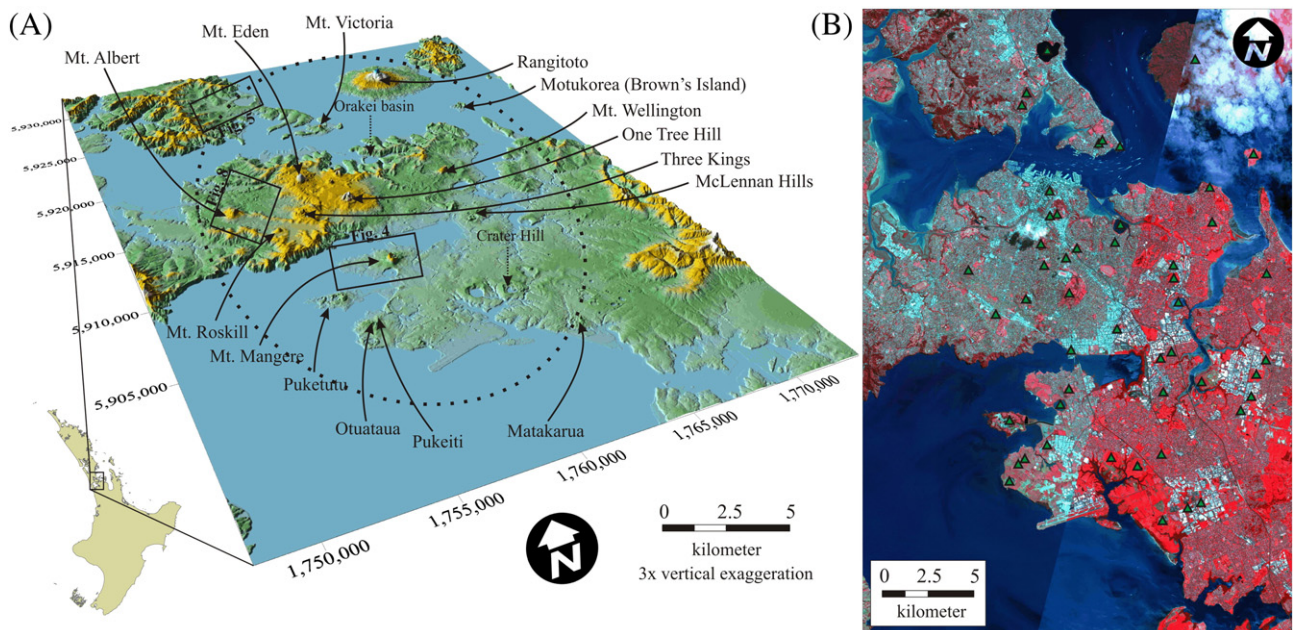


**Fig. 1.** (A) An overview LiDAR-based DEM of the Auckland region with the location of studied volcanic centres. Note that a phreatomagmatic maar volcano, Orakei Basin, and a complex monogenetic volcano with initial phreatomagmatic and late magmatic stage, Crater Hill, both mentioned in the text, are indicated by the dashed arrows. The dashed ellipsoid shows the extent of the Auckland Volcanic Field (after Spörl & Eastwood, 1997). The coordinates are given in New Zealand National Grid metric system. The solid boxes indicate the location of Figs. 4, 5 and 8. (B) Location of the 50 eruptive centres (green triangles) within the City of Auckland overlaid on a false-colour multispectral SPOT-5 satellite image. Note that the areas in grey to green are the urban and heavily populated parts of Auckland, while the red colour shows distribution of vegetated areas, such as forest or park. (For interpretation of the references to colour in this figure legend, the reader is referred to the web version of this article.)

lava flow susceptibility map was created for the City of Auckland using Geographical Information System (GIS).

## 2. Geological setting

Localised intraplate basaltic volcanism formed at least two large concentrations of monogenetic volcanic fields in the North Island, New Zealand (Briggs et al., 1994; Cook et al., 2005; McGee et al., 2011) namely in the Auckland Region comprising Okete Basalts (2.69–1.80 Ma), the Ngatutura Basalts (1.83–1.54 Ma), the South Auckland Volcanic Field (1.59–0.51 Ma), and the Auckland Volcanic Field (0.25–0.0006 Ma) as well as in the Northland Region including longer-lived (9.7–0.0013 Ma) volcanic field near Whangarei and the Bay of Islands. In the Auckland Region, volcanism appears to have migrated from the south to the north at the rate of 55 km/Ma forming clusters of volcanoes (Briggs & McDonough, 1990; Briggs et al., 1994; Hodder, 1984; Spörli & Eastwood, 1997). The AVF is the most recently formed part of this basaltic magmatic system in the North Island. A wide range of radiocarbon, K–Ar and Ar–Ar ages suggests the earliest eruptions took place about 0.25 Ma ago, while the youngest built up a scoria cone complex with associated lava flows about 504 and 553 years BP, Rangitoto (Bebbington & Cronin, 2011; Lindsay et al., 2011; Molloy et al., 2009; Needham et al., 2011). The field is located directly above a boundary between continental terrains of the New Zealand basement, inferred to be the source of a strong NNW–SSE trending geophysical anomaly known as Junction Magnetic Anomaly (JMA). The JMA is anomalously wide beneath Auckland, possibly reflecting intraplate crustal extension behind (200–250 km) the presently active arc system, Taupo Volcanic Zone, of the central North Island (Cassidy & Locke, 2010; Kermode, 1992; Von Veh & Nemeth, 2009).

According to the present eruption age model, the volcanism shows “pulsing” or “flare-up” in rates of activity (Bebbington & Cronin, 2011; Molloy et al., 2009). Based on tephra chronostratigraphy and existing dates from single eruption centres, Bebbington and Cronin (2011) estimated the current hazard at Auckland of 0.0002 events/yr, which decreases over the next 5 ka if quiescence continues. The overall shape of the field is elliptical with its long axis showing a NNW–SSE orientation (Briggs et al., 1994; Spörli & Eastwood, 1997).

The AVF is covered and intercalated with Late Pleistocene alluvial sand, mud and swamp deposits that contain thin tephra horizons from the Taupo Volcanic Zone caldera volcanoes to the south. It is built mostly on a substrate of Early Miocene (e.g. Waitemata and Waitakere Groups) sandstone, mudstone, conglomerate, sand and rare limestone (Edbrooke et al., 2003; Kermode, 1992). The youngest country rocks, including weakly consolidated sand, mud and silt, have played an important role in determining the nature of volcanic eruption styles in the AVF (Allen et al., 1996; Houghton et al., 1999). Initial eruptions at a given centre were mostly characterised by some degree of phreatomagmatic fragmentation, which produced fall and pyroclastic density current deposits. Some volcanoes produced only pyroclastics from phreatomagmatic eruptions, e.g. the Orakei maar (Fig. 1), however, many transitioned to magmatic behaviour, producing scoria cones, spatter cones and lava flows (Allen & Smith, 1994; Hayward et al., 2011; Houghton et al., 1996). This change from initial, ‘wet’ phreatomagmatic toward more ‘dry’ magmatic fragmentation style is particularly common in the AVF (Houghton et al., 1999) and also noted from other monogenetic volcanoes elsewhere (Kereszturi et al., 2011; Martí et al., 2011; Németh et al., 2008). The occurrence of lava flows is mostly related to these transitions, which may have resulted from a reduction in influx of groundwater to the eruption site

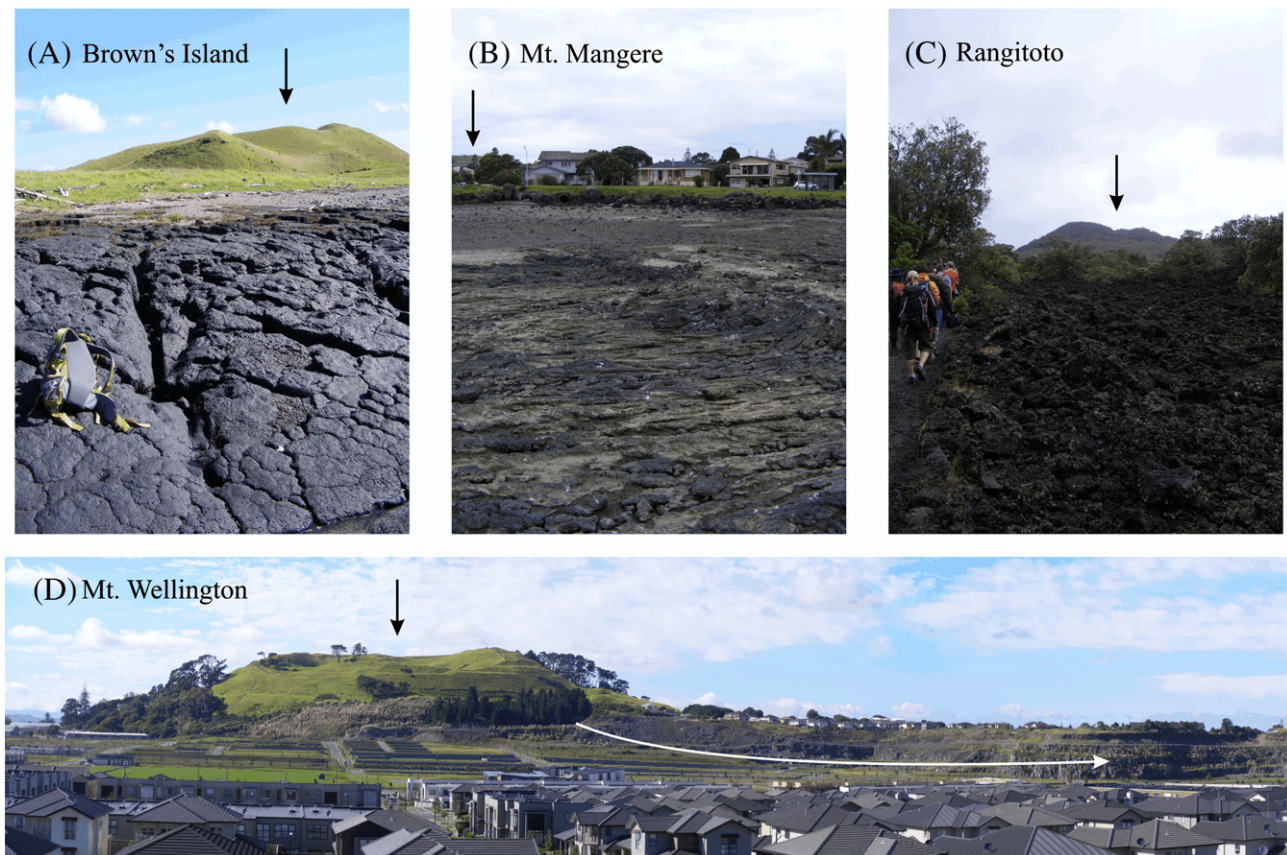


**Fig. 2.** Field photographs illustrating examples of preserved lava flow surfaces and their source scoria cones (black arrows). (A) Aa lava flow surface preserved in the coastal area of Motukorea. (B) Pahoehoe surface related to the Mt. Mangere scoria cone. (C) Fresh aa lava flow from the youngest eruption centre, Rangitoto. (D) Overview photo of the Mt. Wellington scoria cone and its basaltic lava flow exposed due to extensive quarrying. Note that the white arrow indicates the direction of the lava flow.

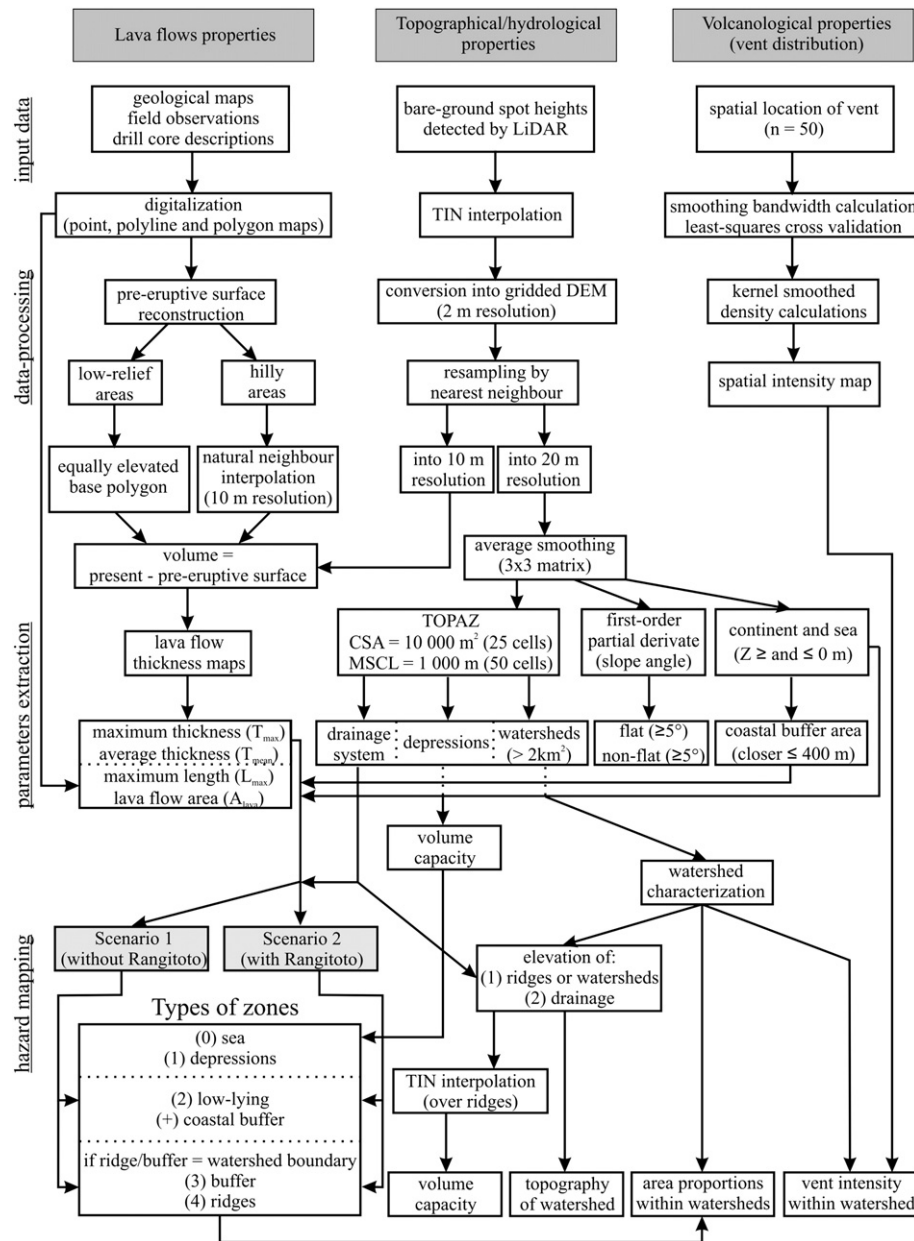


Fig. 3. Flow diagram for input data, data processing and results.

and/or development of stable conduit conditions (Houghton et al., 1999). The late-stage lava flows either filled the crater area formed during the initial phreatomagmatic phase, e.g. Crater Hill (Houghton et al., 1999), or flowed radially away from the vent, e.g. Rangitoto (Needham et al., 2011). In other cases, flows emerged from the foot of scoria cones, e.g. Mt. Wellington (Fig. 2). The lava flows in Auckland are mostly aa in type although at least a few pahoehoe flows also occur (Fig. 2).

### 3. Materials and methods

#### 3.1. LiDAR survey and DSM preparation

Spot heights were obtained by Fugro Spatial Solutions and New Zealand Aerial Mapping Limited companies for the Auckland City Council using two different types of aircraft-mounted LiDAR sensors. A Leica Airborne Laser Scanner 50 (ALS50) and an Optech Airborne Laser Terrain Mapper 3100-EA (ALTM3100) were used in surveys in 2005–2006 and

2008, respectively. Two types of surveys were carried out in each of these years, for urban/intertidal and for rural areas, with different LiDAR settings. The survey for the urban and intertidal (captured at low tide) areas was carried out with an average flight height of 1330 m and 1200 m above ground level at 150 (or 77.1 m/s) and 130 knots (or 66.8 m/s), respectively. These two LiDAR sensors operated between 73 kHz and 70 kHz pulse repetition frequency and 39 and 40 Hz scanning frequency with scanning half-angle of  $\pm 20^\circ$  and  $\pm 22^\circ$  resulting swath widths of 960 m and 968 m, respectively. The accuracy of the LiDAR scanners, without GPS errors, are estimated at  $0.20 \text{ m} \pm 1 \sigma$  horizontally and  $0.15 \text{ m} \pm 1 \sigma$  vertically for the Leica ALS50, while  $0.21 \text{ m} \pm 1 \sigma$  (calculated as  $1/5500 \times \text{flight height in m}$ ) horizontally and  $0.11 \text{ m} \pm 1 \sigma$  vertically for the Optech ALTM3100. The mean ground point density was about 1 point per  $\text{m}^2$ . The rural survey was carried out with average flight heights of 2000 m above ground level at 150 knots (or 77.1 m/s) using the Leica ALS50. The sensor setting was 54.8 kHz pulse repetition frequency, 31 Hz scanning frequency with a scanning half-angle of  $\pm 20^\circ$ . This resulted in a

1455 m swath width. The scanning accuracy was  $0.25 \text{ m} \pm 1 \sigma$  horizontally and  $0.2 \text{ m} \pm 1 \sigma$  vertically. The mean ground point density ranged between 0.04 to 0.15 point/m<sup>2</sup> over areas, such as Rangitoto, Motutapu and Motukorea Islands (Fig. 1). Post-processing including filtering and bare-earth point detection of the point cloud was performed by the data provider, Fugro Spatial Solutions (<http://www.fugrospatial.com.au/>).

In the construction of the DSM, only bare-ground spot heights (last returns) were used. Spot heights on buildings and other anthropogenic features were removed, which decreased the original point density to 0.5 point/m<sup>2</sup>. The DSM was created by the Triangulated Irregular Network (TIN) method and subsequently converted into a grid-based DSM with a  $2 \times 2 \text{ m}$  grid cell size (Fig. 3). To enable ready calculations on this dataset, the original 2 m resolution LiDAR DSM ( $12\,785 \times 18\,366$  cells) was resampled into a 10 m resolution for the volume calculations and 20 m resolution for the hydrologic channel extraction by the nearest neighbour method (Fig. 3). Before hydrologic channel extraction, the DSM was smoothed by an average  $3 \times 3$  ( $60 \times 60 \text{ m}$ ) moving window in order to avoid noise, such as due to vegetation filtering, and enhance computation time (Fig. 3).

### 3.2. Lava flow parameters

During a monogenetic eruption, multiple lava flows (or smaller lava lobes) can form which usually pile on top of each other forming sequences of lava flows (Self et al., 1998; Wantim et al., 2011). In the present study, the final size and dimension of lava flows were measured and treated as a single unit, regardless of whether or not they were formed from multiple smaller lava flows (Fig. 4). In addition, just those lava flows were considered which are visible in the field, having mappable boundaries. There are a few buried lava flows by Holocene sediments and/or volcanics, such as lava flow from Mt. St. John or Green Mountain, but they are discarded from the calculation because of the high uncertainty in their parameterisation.

The polygon of each lava flow was determined on the basis of previously published geological maps (Hayward et al., 2011; Kermode, 1992), aerial photographs and field observations (Figs. 3 and 4). The area of the lava flow ( $A_{\text{lava}}$ ) was derived directly from the area of the digitised polygon (Fig. 4). The length of the lava flows ( $L_{\text{max}}$ ) was calculated from the point maps at equal spacings of 0.5 m, which were converted from the boundary lines of each lava flow. The centre point of each source volcano was defined as a centre point of the local minima (i.e. last closed contour line at the crater bottom of each edifice) or edifice centre if a crater is not present. This was digitised manually from the contour maps with 1 m intervals derived from LiDAR DSM (Fig. 4). The  $L_{\text{max}}$  was calculated between the source point and the lava flow maximum extremity as a vector (Figs. 3 and 4). The volume ( $V_{\text{lava}}$ ) for those volcanoes located on flat areas or forming individual islands/peninsulas such as Mt. Mangere, Rangitoto, Motukorea (Brown's Island), Puketutu, Pukeiti, Otutaua, Matarua and Mt. Victoria was calculated as a difference between the present DSM and an equal base height (i.e. plane). For the rest of the cones, Mt. Roskill, Mt. Eden, Three Kings, Mt. Albert, One Tree Hill and Mt. Wellington, the volume was defined as the difference between the present 10 m DSM and a reconstructed pre-eruptive surface beneath the volcanics (Fig. 4 and Table 1). The pre-eruptive surface was interpolated from spot heights with elevation of the contact of lava flow and the underlying non-volcanic strata derived from drill core points ( $n = 488$ ) and field observations ( $n = 26$ ). The spot height data was used to interpolate a 10 m resolution DEM by using natural neighbour interpolator. Volumes in both cases were determined on a cell basis:

$$V = \sum [(Z_{\text{present}} - Z_{\text{bottom}}) \times \text{AREA}] \quad (1)$$

where  $Z_{\text{present}}$  is the elevation of the LiDAR DSM (i.e. present surface), the  $Z_{\text{bottom}}$  is the reconstructed pre-eruptive surface DEM beneath the lava flows, the AREA corresponds to the grid cell's area (in this case

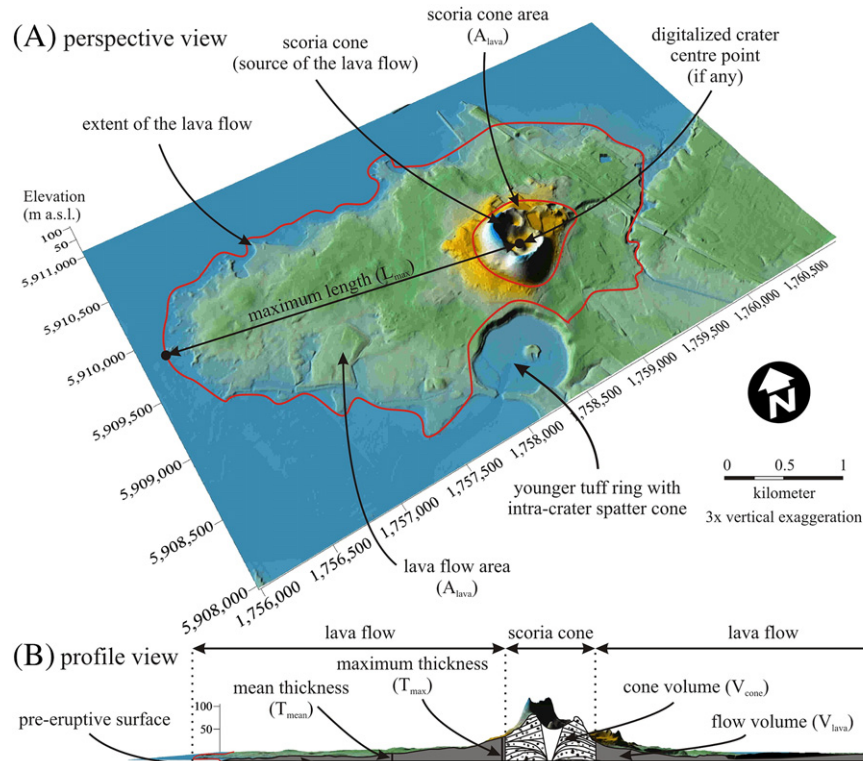


Fig. 4. Perspective (A) and profile (B) views of morphometric parameters of lava flows applied in this paper visualized on the Mt. Mangere volcano (for the detailed location see Fig. 1).

**Table 1**

Summary of morphometric parameters for the studied fifteen lava flows. Note that the volumes of scoria cones were calculated from the basement. The basement was represented either by an equally elevated plane ("Equal") or by an interpolated paleosurface based on the drill core data ("Surface").

N#	Location	Age (ka)	Length (m)		Thickness (m)		Area (m <sup>2</sup> )			Basement height (m)	Bulk volume (m3)		
			L <sub>min</sub>	L <sub>max</sub>	T <sub>max</sub>	T <sub>mean</sub>	Cone	Flow	Total		V <sub>lava flow</sub>	V <sub>cone</sub>	V <sub>total</sub>
1	Pukeiti	117.6 ± 53.4	106.7	762.7	20.7	8.4	35,900	501,800	537,700	equal (=0)	4,265,202	770,959	5,036,161
2	Otuataua	41.4 ± 0.4	149.4	964.5	30.8	14.3	81,500	482,100	563,600	equal (=0)	6,937,735	1,920,211	8,857,946
3	McLennan Hills	40.1 ± 1.2	263.2	1,730.1	29.2	10.3	261,800	1,582,800	1,844,600	equal (=0)	16,333,328	7,077,218	23,410,546
4	One Tree Hill	34.9 ± 0.7	1,359.1	4,403.7	80.8	22.7	374,800	15,292,800	15,667,600	surface	347,362,933	28,456,852	375,819,785
5	Brown's Island	33.7 ± 0.8	150.4	1,155.6	18.3	3.4	144,800	852,900	997,700	equal (=−2)	2,971,052	4,314,795	7,285,847
6	Mt. Albert	32.8 ± 0.5	596.9	2,320.6	34.3	8.3	425,700	3,322,700	3,748,400	surface	27,647,490	15,339,485	42,986,975
7	Puketutu	31.9 ± 0.3	230.0	1,793.7	30.1	6.1	163,600	1,677,200	1,840,800	equal (=0)	9,077,513	5,011,146	14,088,659
8	Mt. Victoria	31.1 ± 0.1	188.7	754.7	29.4	10.8	136,800	304,800	441,600	equal (=0)	2,905,802	6,029,926	8,935,728
9	Mt. Roskill	30.5 ± 1.2	219.1	2,463.2	29.3	8.2	241,100	1,392,500	1,633,600	surface	11,513,967	6,865,428	18,379,395
10	Three Kings	28.8 ± 0.3	411.7	5,723.8	46.3	14.1	480,300	6,086,600	6,566,900	surface	85,008,373	14,308,042	99,316,415
11	Mt. Eden	28.4 ± 0.3	902.6	2,175.8	76.3	26.9	405,000	5,136,000	5,541,000	surface	138,656,128	29,804,539	168,460,667
12	Matakara	27.0 ± 0.6	90.6	732.6	38.6	15.9	30,800	542,200	573,000	equal (=0)	8,637,999	1,008,765	9,646,764
13	Mt. Mangere	21.9 ± 0.4	557.6	2,699.3	29.3	8.5	873,600	4,344,900	5,218,500	equal (=0)	36,099,442	34,896,667	70,996,109
14	Mt. Wellington	10.5 ± 0.1	369.9	6,525.8	48.8	20.2	262,600	5,981,000	6,243,600	surface	127,521,507	15,130,206	142,651,713
15	Rangitoto	0.5 ± 0.0	2,241.8	3,677.0	180.5	43.8	416,400	24,686,000	25,102,400	equal (=−3)	1,083,230,686	81,750,692	1,164,981,378
MEAN without Rangitoto (Scenario 1)			2,443.3		38.7	12.7	279,879	3,392,879	3,672,757	MEAN	58,924,176	12,209,589	71,133,765
MEAN with Rangitoto (Scenario 2)			2,525.5		48.2	14.8	288,980	4,812,420	5,101,400	MEAN	127,211,277	16,845,662	144,056,939
SUM											1,908,169,157	252,684,931	2,160,854,088

10 × 10 m = 100 m<sup>2</sup>). The volume values were not corrected for vesicularity, thus they are bulk volumes. From the residual maps, the maximum (T<sub>max</sub>) and mean thickness (T<sub>mean</sub>) of the lava flow were calculated (Figs. 3 and 4). Error in the volume calculations can be associated with (1) surface processes including erosion after the formation of the lava flows and anthropogenic activity, such as quarrying, (2) data capturing techniques, such as laser positioning, angle of view, distance from the surface and the laser and topography (Aguilar et al., 2005; Favalli et al., 2009a; Pollyea & Fairley, 2012; Su & Bork, 2006) as well as (3) processing of the raw data including systematic correction, gridding, subsequent smoothing or resampling (Aguilar & Mills, 2008; Favalli et al., 2010). In this study, the applied low, average smoothing and resampling from 2 m to 10 m resolution may introduce some modification of the volume and thickness calculations. To express the expected differences and data modification introduced by these post-processing techniques, the parameters derived from these two data sets were crosschecked. The smallest (Pukeiti) and largest (Rangitoto) volcanoes were selected for comparison. The differences between the 2 m and 10 m resolution DSMs were ≤16 429 m<sup>3</sup> (0.001%) and 903 m<sup>3</sup> (0.02%) for the volume and 0.01 m (0.1%) for thickness, respectively. Finally, the overall accuracy of the LiDAR DSM is in the dm range, thus only one decimal place was considered in the calculations and results, except for the volume calculations because there were converted from m<sup>3</sup> into km<sup>3</sup>.

### 3.3. Hydrological channel extraction

Hydrological characteristics and associated features, such as valleys and ridges and their orientations, can be used to describe the terrain (Bonne et al., 2008; Favalli et al., 2009b; Jordan, 2003; Jordan & Schott, 2005; Moore et al., 1991; Székely & Karátson, 2004). The theoretical drainage system (Fig. 3) was extracted from the resampled, 20 m resolution LiDAR DSM using TOPographic PARAMeteriZation (TOPAZ) application developed by Garbrecht and Martz (1995). The methods behind the TOPAZ include the D8 method (Douglas, 1986), the down-slope flow routing (Morris & Heerdegen, 1988) and the critical source area method (Mark, 1984). Interpolation noise, such as isolated pits or depression cells or flat cells, may distort the final results of drainage extraction (Costa-Cabral & Burges, 1994; Garbrecht & Martz, 1997; Jensen & Domingue, 1988). TOPAZ uses a breaching algorithm that detects local minima in a DSM or in a DEM on a 5 × 5 cell matrix (Garbrecht & Martz, 1995). This algorithm systematically lowers the elevation along the rim of the depression and then fills depressions by modification of cell elevation (Martz & Garbrecht, 1999). To extract

drainage patterns from a DSM or from a DEM by the TOPAZ, two input parameters are required (Fig. 3). The Critical Source Area (CSA) defines the drainage channel as raster cells that have an upstream area greater than the user-defined threshold value (Garbrecht & Martz, 1995; Mark, 1984; Martz & Garbrecht, 1992). The Minimum Source Channel Length (MSCL) defines the minimum length of individual channels extracted from the DSM or DEM (Garbrecht & Martz, 1995). In the present study, the CSA chosen was 10 000 m<sup>2</sup> (25 cells), and the MSCL chosen was 1000 m (50 cells), respectively (Fig. 3). These values are high enough to extract a dense drainage which is a good basis of further re-interpolation (see details later), while the 1000 m MSCL value allows extracting only longer channels which are potentially large enough to control the pathway(s) of future lava flows.

### 3.4. Topographic classification of zones subject to lava flow inundation

The present topography was classified as (i) sea, (ii) depressions, (iii) low-lying areas, (iv) a buffer zone and (v) ridges (Figs. 3 and 5). Due to the coastal location of Auckland, the total area covered by sea is also an important class, but the proper lava flow pathway prediction under this area is uncertain due to the lack of high-resolution bathymetric data. In this investigation, the sea was defined in a raster-based environment as those areas that are characterised elevation ≤0 m a.s.l. (Figs. 3 and 4).

The local minima (i.e. topographic depressions), in which a cell has surrounding cell with higher elevation values, are most likely to be filled by lava flows. To identify and delimit them, a sink-filling algorithm was used (Jensen & Domingue, 1988). These areas are assumed to be the most susceptible to inundation by a lava flow sourced from a distance ≤ L<sub>max</sub> (6.5 km; Fig. 5). The low-lying areas are referred to here as those parts of the field which are currently characterised by smooth surfaces with low elevation differences (<T<sub>mean</sub>; 12–14 m), hence they could be buried easily by a lava flow sourced ≤ L<sub>max</sub> (6.5 km) and having an average thickness (Fig. 5). To delimit these areas, the theoretical drainage system was used as a basis with the assumption that future lava flows will follow the topography and therefore the drainage system. To delimit zones, such as low-lying, buffer and ridges, the cell elevation values along drainage channels as local lowest points, were increased by the values of T<sub>mean</sub> (Fig. 5), similar to Jordan (2007a). The cell values (present elevation + T<sub>mean</sub>) were then converted into points which were used to construct a new surface by TIN interpolation (Fig. 5). The constructed TIN surface was converted into gridded DEM with 10 m resolution and extracted from the original DSM. Those areas below

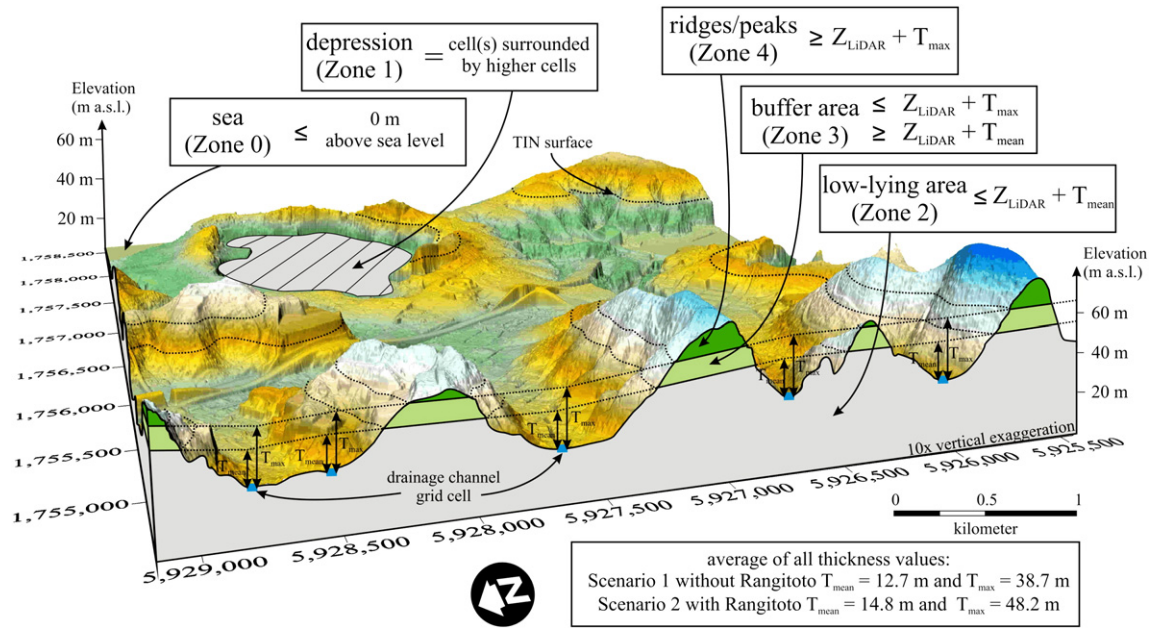


**Fig. 5.** Definitions of susceptibility zones (sea, depressions, low-lying area, buffer and ridges/peaks) identified in the City of Auckland visualised on the northern part of the City (for the detailed location see Fig. 1). The largest depression in the figure is the Lake Pupuke, generated by series of phreatomagmatic eruptions.

the interpolated TIN surface are defined as low-lying areas that could be affected by a future lava flow from a source closer than  $L_{max}$ . The delimitation of the buffer zone was constructed using the same technique, but substituting  $T_{mean}$  with  $T_{max}$  values (38–48 m; Fig. 5). The rest of the area (i.e. above the buffer zone), is locally above the valley bottoms by  $T_{max}$ , therefore they are characterised as ridges. The advantage of this method is that it is adaptive, and uses the local lowest values of the surface as a basis to construct topographic classification/hazard zonation.

The definitions of this classification are based on (i) the topographical properties and (ii) the lava flow parameters introduced above. The morphometric parameters of the lava flows, such as thickness, lie within a narrow range, but there is an outlier value associated with the massive lava field of Rangitoto (Fig. 6). Thus, this asymmetry of the thickness data means that the definitions of the low-lying, buffer and ridge zones could differ significantly. To handle this asymmetry, two scenarios were calculated. Scenario 1 uses the morphometric parameters without Rangitoto values, while Scenario 2 contains all of the morphometric values of the field (Fig. 3 and Table 1).

Additional, significant features of the present topography (e.g. flat areas) were also detected using slope-angle maps (Fig. 3). Here, flat areas were defined as having a  $\leq 5^\circ$  slope angle (Fig. 3). Generally, these flat areas would favour the broad spread of lava flows over the topography (Favalli et al., 2009b). Slope was calculated by using an unweighted, third order finite difference filter ("Prewitt" filter), which gives more general "smoothed" slope values. This linear filter applies a first-order trend surface fitted to the cell values on a  $3 \times 3$  moving window by least-squares method (Jones, 1998; Jordan, 2007b; Sharpnack & Akin, 1969). The slope angle in a grid-based environment is formally written as:

$$\text{SLOPE} = \arctan \sqrt{f_x^2 + f_y^2} \quad (2)$$

in which the first derivatives are calculated as  $f_x = (Z_3 + Z_6 + Z_9 - Z_1 - Z_4 - Z_7) / 6\Delta X$  and  $f_y = (Z_1 + Z_2 + Z_3 - Z_7 - Z_8 - Z_9) / 6\Delta Y$ , where  $Z_1 - Z_9$  correspond to the cell elevation read from the top left corner to the bottom right corner in a  $3 \times 3$  matrix, and  $\Delta X$  and  $\Delta Y$  are the grid cell size along the two main principal directions.

Other point-like features, such as valley conjunctions and watershed outlets, were also digitised manually, with the value of upstream areas taken from the theoretical drainage system map. The valley conjunctions possibly represent an increased likelihood of lava inundation from multiple directions (i.e. from different valleys), if the eruption takes place within the upstream area. An outlet point along the coastal area may represent a location with increased likelihood of explosive sea water/lava interaction associated with littoral cone formation (Mattox & Mangan, 1997). A 400 m-wide coastal-hazard zone was thus created around the coastal regions (Fig. 3) based on the dimensions of littoral cones (up to 400 m in width (Jurado-Chichay et al., 1996)). The sea was defined in a raster-based environment as those areas that are characterised elevation  $\leq 0$  m a.s.l. Thus, the coastal buffer zone was constructed from this boundary between the land and sea using raster-based distance calculation.

### 3.5. Watershed characteristics

Topography, especially ridges that divide watersheds, is highly effective in controlling lava flow emplacement (Bonne et al., 2008). Adapting this concept, the watersheds that are large enough to host a future eruption ( $\geq 2 \text{ km}^2$ ) were extracted, noting that small watersheds can be easily overtopped or destroyed by vent opening eruptions or vent migrations (Fig. 3). Taking the fact that an average monogenetic eruption (excluding tephra fall) rarely impacts a circular area larger than  $\sim 0.75 \text{ km}$  in radius (Magill & Blong, 2005a), the minimum area of each event would be  $\geq 2 \text{ km}^2$  (i.e.  $\geq 4500$  cells). Each watershed defined can be evaluated in terms of its future susceptibility to eruptions by calculating the number of past eruption onsets that occurred in it (Fig. 3). Kernel smoothed density methods, based on the location of all past eruption centres including all eruption centres ( $n=50$ ) were used to evaluate a spatial intensity. Two-dimensional, symmetric Gaussian kernel density estimates were used (Connor & Hill, 1995):

$$\lambda(s) = \frac{1}{2\pi h^2} \sum_{i=1}^n \exp \left[ -\frac{1}{2} \left( \frac{d_i}{h} \right)^2 \right] \quad (3)$$

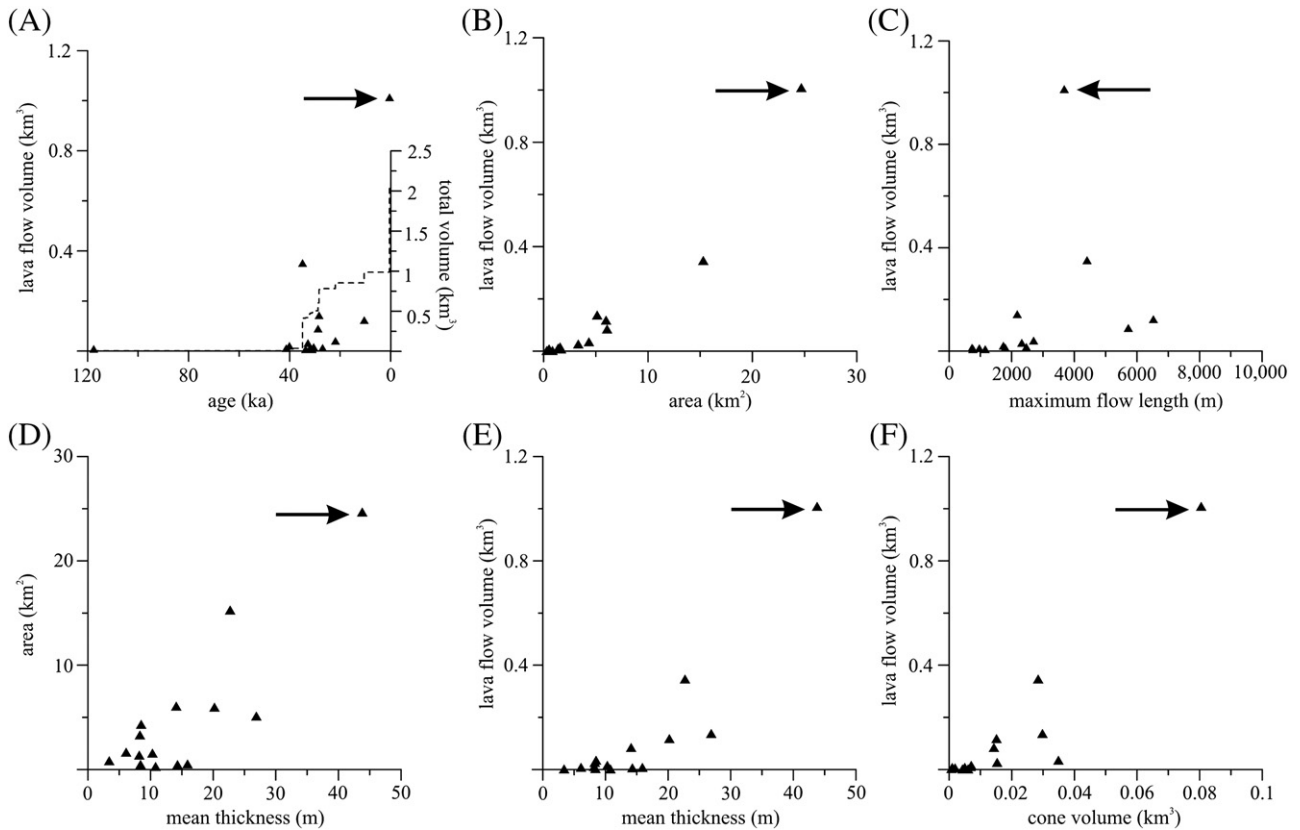


**Fig. 6.** Graphs of the main morphometric parameters of lava flows. Age estimates are from [Bebbington and Cronin \(2011\)](#). Note that the black arrows indicate the morphometric values of Rangitoto volcano.

where  $d_i$  is the distance from the point of interest,  $s$ , to the vent location,  $n$  is the number of vents, and  $h$  ( $=2.42$  km) is the smoothing bandwidth. The bandwidth was determined by least squares cross validation ([Duong, 2007](#)). To approximate probabilities of future eruptions and possible lava flows within watersheds, the spatial intensity values were averaged within the area of each watershed and ranked ([Fig. 3](#)).

Other characteristics were calculated for each watershed, such as area of depressions, low-lying, buffer and ridge areas (in  $\text{km}^2$  and %) for the scenarios, average number and volume of lava flows within a watershed, perimeter and average elevation of drainage as well as watershed border and volume capacity ([Fig. 3](#)). The raster-based maps of each watershed were converted into vector-based polygon and subsequently polylines. Such polylines were rasterised with the same spatial resolution (i.e. 20 m), in order to extract elevation values along the watershed boundaries. The elevation values were also extracted along the drainage systems. For both cases, mean, median and standard deviations were calculated in order to characterise the topographical variations within a watershed and between watersheds ([Fig. 3](#)). The hosting capacities of the watersheds were established by Eq. (1) between present LiDAR DSM and a surface constructed by TIN interpolation from the elevation values along the present ridgelines, similar to [Jordan \(2007a\)](#).

## 4. Results

### 4.1. Characteristics of past lava flows

The lava flows examined in the present study are  $\leq 0.1$  Ma old, thus the erosion-related modification is negligible as the rocks are still relatively fresh and erosion resistant. Some modifications may be expected from anthropogenic processes, such as quarrying ([Fig. 2D](#)). The largest portion

of lava flow was quarried away from the Mt. Wellington reducing the original volume by  $0.008 \text{ km}^3$  ([Fig. 2D](#)). From the fifteen preserved lava flows ([Fig. 1](#) and [Table 1](#)), the maximum length of the AVF lava flows range between 0.7 km (Mt. Matarua) and 6.5 km (Mt. Wellington; [Fig. 5](#)), while the average is 2.5 km ([Table 1](#)). The longest flow of Auckland is, however, from the Mt. St. John volcano with the total length of about 10 km ([Eade, 2009](#)). Due to the limited knowledge about its exact path, it was discarded from the calculations. Interestingly, the exceptionally large eruptive centre of Rangitoto did not produce the longest flows ([Table 1](#)) because they were concentrically emplaced around the vent and flowed over a flat basal topography. The average area invaded by a single AVF eruption centre is around  $5.1 \text{ km}^2$  including  $4.8 \text{ km}^2$  lava flow and  $0.3 \text{ km}^2$  scoria cone area. These areas range from  $<0.5 \text{ km}^2$ , (e.g. at Mt. Victoria and Pukeiti) to  $24.6 \text{ km}^2$  and  $15.2 \text{ km}^2$  for the Rangitoto and One Tree Hill centres, respectively ([Table 1](#)).

Bulk total edifice volumes (cone + lava flow), excluding basal phreatomagmatic deposits and distal tephra, show high variability from  $0.005 \text{ km}^3$  (Pukeiti) up to  $\sim 1 \text{ km}^3$  (Rangitoto) ([Table 1](#)). From these, the most significant portions are preserved as lava flows. Other large lava flows include: One Tree Hill ( $0.34 \text{ km}^3$ ), Mt. Eden ( $0.13 \text{ km}^3$ ), Mt. Wellington ( $0.12 \text{ km}^3$ ) and Three Kings ( $0.08 \text{ km}^3$ ). The maximum and mean thicknesses of lava flows from individual centres are between 18.3–180.5 m and 3.4–43.8 m, (from Motukorea to Rangitoto) ([Table 1](#)). Based on the past effusive activity, an average AVF lava flow is characterised by a mean thickness of 14.8 m, while the mean maximum thickness is 48.2 m. If the fact that the Rangitoto is an outlier volcano in terms of eruption duration ([Needham et al., 2011](#)), geochemistry ([McGee et al., 2011](#)) as well as size were considered, and it was excluded from the calculations, the mean and mean maximum thickness values decrease to 12.7 m and 38.7 m, respectively ([Table 1](#)). The average volume of the fifteen lava flows measured here is

0.127 km<sup>3</sup> which can be related to an average edifice with a volume of 0.016 km<sup>3</sup> measured from the basement.

No distinct trends can be seen in lava flow volume as a function of lava flow length (Fig. 5), because many large flows related to the Rangitoto eruption spread widely on flat topography, thus the maximum length is only 3.6 km (Table 1). On the other hand, there is a correlation between flow volumes and their areal extent meaning that the lava flows were mostly emplaced freely over the topography (Fig. 5). Volumetric evolution in the field considers total lava flow and scoria cone volumes (excluding the eruption products of phreatomagmatic eruption and ash dispersion) shows a rapid increase due to the large size of the last eruption, Rangitoto.

#### 4.2. Characteristics of present topography

The area examined (793 km<sup>2</sup>; Fig. 1) is slightly more than twice that of the area of the AVF, about 336 km<sup>2</sup> (Spörli & Eastwood, 1997). From the study area, around 40% is covered by the sea or is intertidal (326 km<sup>2</sup>), and because this is not inhabited, it was excluded from our analysis. Based on present topography, the study area can be subdivided into two significantly different areas: (i) a valley–ridge-dominated northern/central region; and (ii) the plain-dominated southern region (Fig. 1). The northern part is characterised by low ridges composed of sandstone (Waitemata Fm.), whereas the southern part is mostly covered by Late Pleistocene–Holocene alluvium, peat and marine sands and mud (Edbrooke, 2001; Kermode, 1992). The extracted drainage system is characterised by having a dense channel system (0.7 km/km<sup>2</sup>). The average distance between individual channels is 374 m (median = 321 m) and 73% of the channels are <500 m away from their neighbouring ones. This dense drainage provides a good detailed basis to re-model the topography during the secondary TIN interpolation and thus to calculate inundated areas by an average lava flow.

As described above, the classification of the topography into zones (sea, depressions, low-lying areas, buffer area and ridges) is based on the mean thickness of past lava flows. Due to the outlier values of Rangitoto, two scenarios were used (Scenario 1 without, while Scenario 2 with Rangitoto). From the zones above, the sea and depressions are the same for both scenarios.

The depressions (Fig. 5) have a maximum depth of 49.4 m, e.g. the quarry near Three Kings (Fig. 1). The rest of the depressions are shallower (average depth of 1.8 m) and 70% of them are <1.5 m deep. Most of these are small-scale pits due to rapid changes in topography, detection error or interpolation noise. There are very few natural depressions, such as maar craters. The total area of depressions is around 45.2 km<sup>2</sup>, but from these only 9 km<sup>2</sup> (1.1% of the total area) is inferred to represent 'real' depressions (i.e. areas larger than a few grid cells in width; Fig. 6). The total volume of these depressions that can be invaded by future lava flows is about 0.062 km<sup>3</sup>.

The low-lying zone (Fig. 5) covers an area of 300 km<sup>2</sup> (38 %) and 319 km<sup>2</sup> (40 %), without and with Rangitoto lavas, respectively (Table 2). Consequently, an overwhelming proportion of the AVF is characterised by not distinct topographical difference, thus a future flow with an average thickness cannot be fully channelised by the topography. In both scenario cases, this zone has slope angle dominantly <5° (253/265 km<sup>2</sup> or 84/83% of the area). The flat areas are mostly located in the southern part of the volcanic field.

The 'buffer' zone (Fig. 5), between low-lying and ridge zones encompasses 121 km<sup>2</sup> and 118 km<sup>2</sup>, with and without Rangitoto (Table 2), respectively, or ~15% of the total study area. This area mostly coincides with sandstone ridges made up by Waitemata sediments and minor areas of scoria cones. The largest differences in area between scenarios can be found in the case of the most elevated parts, i.e. ridges (Table 2), with 35 km<sup>2</sup> (4 %) excluding Rangitoto and 19.7 km<sup>2</sup> (2%) including it. These areas should be relatively safe, unless a future eruption takes place on the ridges.

In parallel with the lava susceptibility zone classification, the largest watersheds (i.e. 2 km<sup>2</sup>), were also extracted in order to characterise their properties, such as size, hosting capacity and boundary heights, and then ranked based on the spatial intensity of past eruptions. The total number of 'large' watersheds is 40, but only 38 have outflow points in the study area (Fig. 7 and Table 3). They range in area between 1.9 km<sup>2</sup> and 30 km<sup>2</sup>. The elevation of cells on the ridges versus those along the drainage channels were extracted from each other to detect those watersheds that are surrounded by low or less significant ridges (possibly  $\leq T_{\text{mean}}$  or  $T_{\text{max}}$ ). These differences were generally larger than an average lava flow thickness (i.e. 14.7 m; Table 1). Nevertheless, there are only 13 watersheds, mostly in the southern part of the field, which are characterised by low watershed boundaries. The volume capacities range from 0.006 km<sup>3</sup> up to 0.475 km<sup>3</sup>, with an average of 0.088 km<sup>3</sup> (Table 3). This number is significantly smaller than an average lava flow volume (i.e. 0.127 km<sup>3</sup>), in the study area. Only 10 valleys are significantly larger than the average lava volume. The averaged spatial intensity within watersheds range from zero (e.g. watershed ID1) to 0.25 (e.g. watershed ID12) vents per km<sup>2</sup> (Fig. 7 and Table 3).

#### 5. Discussion

In the case of active monogenetic volcanic fields, such as the AVF, forecasting of future hazards can be challenging due to the unknown location of the next event, lack of well defined orientation of previous vents, or inapplicability of classical volcano monitoring techniques, such as geochemical or geodetic/deformation (Ashenden et al., 2011; Lindsay et al., 2010). Even with seismology, real-time observation and identification of small-volume magma as it travels towards the surface can be challenging in Auckland due to large anthropogenic background noise and the coarse resolution of monitoring sites (Ashenden et al., 2011). This means that localisation of a future eruption site is only likely to occur within a few hours or days of an eruption. Hence there is a need for establishing a vent location-independent view of lava flow susceptibility that can be applied in any future scenario or modelling study. There have been many recent efforts to understand the nature and behaviour of potential future hazard from a volcanic eruption, earthquakes, tsunamis and landslides, within New Zealand's most densely populated urban area (Allen & Smith, 1994; Bebbington & Cronin, 2011; Edbrooke et al., 2003; Magill & Blong, 2005a; Magill et al., 2005; Molloy et al., 2009; Needham et al., 2011; Samsonov et al., 2010; Smith & Allen, 1993). Most of these studies focused on the impacts of initial vent-opening processes, such as base surge or ash fall, within the city. Knowledge of lava flow susceptibility is an essential addition, because over half of the eruptions in Auckland have produced lava flows or lakes (Allen & Smith, 1994). For example,

**Table 2**  
Differences in the area of hazard zones using two simulated scenarios.

Zone	N# of pixels	Area (m <sup>2</sup> )	Area (%)	Volume capacity (m <sup>3</sup> )
Scenario 1 (without Rangitoto)				
Sea	815,280	326,112,000	41.1	–
1 Depressions	23,044	9,217,600	1.2	62,622,601
2 Low-lying	751,696	300,678,400	37.9	–
3 Buffer	304,371	121,748,400	15.3	–
4 Ridge	88,872	35,548,800	4.5	–
Scenario 2 (with Rangitoto)				
Sea	815,280	326,112,000	41.1	–
1 Depressions	23,183	9,217,600	1.2	62,622,601
2 Low-lying	798,124	319,249,600	40.2	–
3 Buffer	297,206	118,938,000	15.0	–
4 Ridge	49,470	19,788,000	2.5	–
	1,983,263	793,305,200		

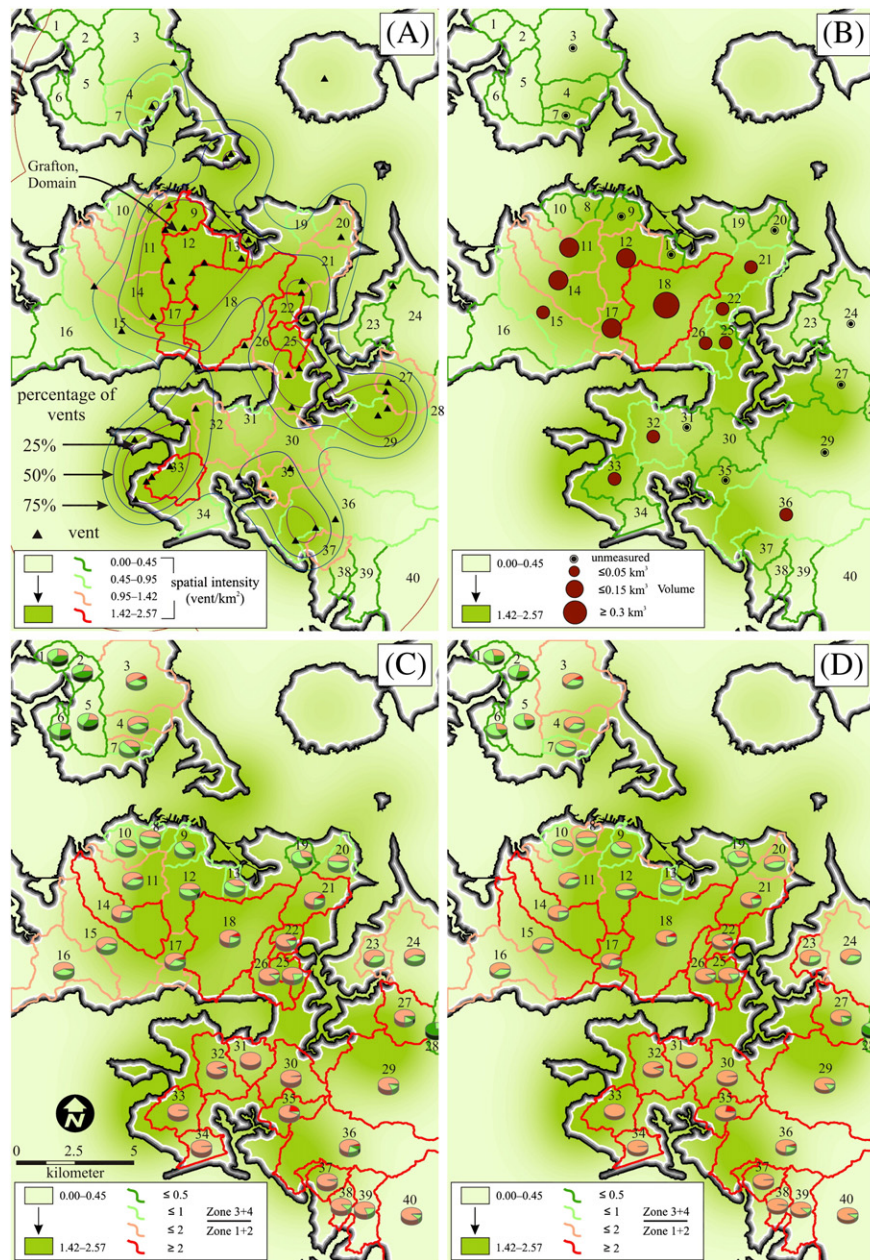


**Fig. 7.** Figure showing the spatial density of the entire field (green background on each map) based on the location of the 50 eruption centres (triangles in A). A 400 m wide zone at the coastline is indicated by black-grey-white lines, see text for explanation. (A) Watershed ranking based on the averaged kernel density. The contour lines (black lines) represent the 25%, 50% and 75% percentage of input point used to estimate the probability density distribution. (B) Watershed ranking based on cumulative volume. (C and D) These two maps show the area portion (pie diagrams) of zones within watersheds for the Scenario 1 (C) and Scenario 2 (D). The colouring of the watershed boundaries shows the ratio between the total areas of buffer (light green) and ridge/peaks (dark green) as well as depressions (red) and low-lying areas (pink). The colours used here are the same as on the lava flow susceptibility map in Fig. 9. (For interpretation of the references to colour in this figure legend, the reader is referred to the web version of this article.)

in the central part of the field, there are remnants of 12 monogenetic volcanoes, of which 10 have lava flows with relatively large dimensions. These parts of the field are also the most densely populated areas of the City.

### 5.1. Lava flow susceptibility

In this study, the topography and morphometry of past lava flows were used to generate a simple map that outlines relative susceptibility to inundation by lava flow associated with a future monogenetic eruption (Fig. 9). One of the major advantages of this assessment is that it is completely vent-location independent, preferable for hazard prediction

in less-frequently erupting monogenetic volcanic fields. The main assumption of this technique to produce lava flow susceptibility maps is that the topography will play the major role in controlling the distribution of lava flows, which has been widely documented elsewhere (Bonne et al., 2008; Favalli et al., 2009b). Based on the lava flow susceptibility map, the potentially safe areas were identified as buffer and ridge zones. The zones in the Fig. 9 only depict lava flow susceptibility from distal sources (closer than  $L_{\max} < 6.5$  km), because near vent accumulation of lava can produce thicker lava accumulations (e.g. Rangitoto) and the vent opening eruption may truncate the topography merging watersheds. A future lava flow may not travel as far as in past examples, up to 10 km (Eade, 2009), because of the high density of buildings especially in the

central parts of Auckland, thus the 6.5 km flow distance is a maximum estimate.

In the AVF, there are two distinct parts of the lava flow susceptibility map (Fig. 9), a northern-central hilly region and a southern flat region. Thus, different flow behaviour is expected over these two areas. The southern parts of the City of Auckland are characterised by watersheds that lack of natural topographical boundaries and that have small differences in elevation between the watershed boundaries and channels (Fig. 9). This implies that future lava flows can easily flow over the topography, affecting multiple watersheds. On this flat terrain dominated by anthropogenic features, such as houses, bridges or roads, the topography-based lava flow forecasting codes could forecast incorrect and unrealistic pathways for future lava flows due to the minimal elevation difference between neighbouring cell values. Such a minimal elevation difference may also be caused by differences in anthropogenic features (e.g. houses), vegetation, errors in the data acquisition or subsequent raw-data processing, such as vegetation filtering and noise reduction. If a future eruption takes place in the southern region of the field, it will likely result in either a landform similar to Rangitoto and/or a phreatomagmatic crater filled by lava flows (Fig. 1). However, its size and geographical extent over the flat topography will vary as a function of total volume of magma and effusion rates involved in the

eruptions. To model such distribution a more effusion rate or viscosity-governed lava flow simulation is needed.

In contrast, most lava flows that have been emplaced during the last 50 ka are situated in the northern and central part of the field, within valleys on the Waitemata paleosurface (Fig. 1). In these regions, the size (i.e. thickness, length, or area) and shape (i.e. elongated or circular) of past lava flows were strongly governed by the properties of hosting valleys (Fig. 8). The elevation difference between the topographic lows (depressions and valley bottoms) and highs (ridges or hill tops) are large enough to stop or force future lava flows to change direction, and therefore control their geographical extent (Fig. 9). The central and northern parts of the City of Auckland host the majority of the ridges that can be interpreted as relatively safe places from a distal ( $<L_{\max}$ ) future lava flow. Overall, due to the generally low volume host capacity (i.e. lack of depressions) of these watersheds, future lava flows are inferred to either fill their initially hosting watershed rapidly and spill out to neighbouring ones (especially in the southern region), or flow down to the coastal area and enter into the sea, possibly forming littoral cones. The likelihood of overspill of lava from a watershed to another may be low because the volumes beneath the present ridge lines are high, mostly  $>0.12 \text{ km}^3$ , similar to the volume of an average flow of the AVF (Table 3).

**Table 3**  
Properties of large ( $\geq 2 \text{ km}^2$ ) watersheds. The values in bold represent either the smaller topographical differences between catchment rims and drainage than a lava flow with average thickness or those catchment that are limited (i.e. smaller than average lava flow) in volume capacities.

ID	N# of pixels	Area									
		Total	On the map	Scenario 1				Scenario 2			
				Zone 1	Zone 2	Zone 3	Zone 4	Zone 1	Zone 2	Zone 3	Zone 4
Unit	Number	km <sup>2</sup>	km <sup>2</sup>	km <sup>2</sup>	km <sup>2</sup>	km <sup>2</sup>	km <sup>2</sup>	km <sup>2</sup>	km <sup>2</sup>	km <sup>2</sup>	km <sup>2</sup>
1	6193	2,477,200	2,477,600	0	606,800	960,800	909,200	0	720,000	1,144,000	612,800
2	6404	2,561,600	2,562,000	0	475,200	969,600	1,116,400	0	554,800	1,233,600	772,800
3	38,419	15,367,600	14,364,400	1,259,200	7,030,400	5,081,600	990,800	1,259,200	7,630,400	5,067,600	404,800
4	12,098	4,839,200	4,839,600	18,000	2,740,800	1,681,600	399,200	18,000	3,045,200	1,588,400	188,000
5	17,201	6,880,400	6,880,800	0	1,457,600	3,043,600	2,379,200	0	1,696,000	3,794,400	1,390,000
6	4764	1,905,600	1,906,000	1600	422,000	970,000	512,400	1600	518,800	1,099,200	286,400
7	5458	2,183,200	2,183,600	0	814,400	1,067,600	301,600	0	894,800	1,204,800	84,000
8	4938	1,975,200	1,975,600	0	926,800	966,800	80,800	0	1,022,400	952,000	0
9	8074	3,229,600	3,230,000	2,800	1,082,800	1,811,600	332,800	2,800	1,192,000	1,947,200	88,000
10	8169	3,267,600	3,268,000	0	1,220,000	1,905,200	142,800	0	1,392,400	1,875,600	0
11	20,980	8,392,000	8,392,400	405,600	4,742,800	3,042,800	201,200	405,600	5,131,600	2,763,200	92,000
12	21,701	8,680,400	8,680,800	116,400	4,148,400	3,488,800	927,200	117,200	4,483,200	3,690,400	390,000
13	5010	2,004,000	2,004,400	0	807,600	1,101,200	95,600	0	902,800	1,101,600	0
14	28,817	11,526,800	11,527,200	218,000	8,028,800	3,011,200	266,400	267,200	8,482,400	2,634,000	140,800
15	31,834	12,733,600	12,734,000	63,200	7,897,600	4,139,600	633,600	63,200	8,526,800	3,920,000	224,000
16	34,414	13,765,600	12,527,600	13,600	7,135,600	4,714,400	663,200	13,600	7,703,200	4,617,600	192,400
17	10,862	4,344,800	4,345,200	268,000	2,499,200	1,325,200	252,400	268,000	2,732,800	1,214,400	129,600
18	51,174	20,469,600	20,470,000	1,654,000	13,472,800	4,636,400	706,800	1,654,000	14,052,800	4,472,000	291,200
19	5206	2,082,400	2,082,800	0	609,200	1,233,600	240,000	0	687,200	1,374,400	21,200
20	8457	3,382,800	3,383,200	44,000	1,610,000	1,614,000	114,400	44,000	1,861,200	1,472,000	5,200
21	17,073	6,829,200	6,829,600	660,400	4,345,200	1,525,600	298,400	660,400	4,727,200	1,325,600	116,400
22	5863	2,345,200	2,345,600	146,000	1,836,400	326,400	36,800	146,000	1,923,200	250,000	26,400
23	7929	3,171,600	3,172,000	0	2,056,400	1,097,200	13,600	0	2,310,800	856,400	0
24	34,763	13,905,200	12,041,200	42,000	7,066,800	4,326,400	600,000	42,000	7,902,800	3,879,600	210,800
25	7143	2,857,200	2,857,600	8,800	2,210,400	620,000	18,000	8,800	2,358,400	490,000	0
26	12,154	4,861,600	4,862,000	173,200	4,087,200	563,600	37,200	173,200	4,182,000	500,400	5,600
27	18,294	7,317,600	7,318,000	30,400	5,434,400	1,207,200	622,800	30,400	5,632,000	1,202,400	430,000
28	No outlet	–	1,307,600	0	21,200	317,200	969,200	0	30,000	506,400	771,200
29	77,268	30,907,200	26,655,600	133,600	21,762,400	3,695,200	1,063,600	133,600	22,494,000	3,387,200	640,000
30	19,946	7,978,400	7,978,800	202,000	7,752,400	22,000	0	0	202,000	7,764,800	9,600
31	11,860	4,744,000	4,744,400	2400	4,739,600	1200	0	2,400	4,739,600	1200	0
32	17,550	7,020,000	7,020,400	410,400	6,054,000	399,200	156,000	410,400	6,147,200	370,400	91,600
33	14,688	5,875,200	5,875,600	0	5,522,800	99,600	0	0	5,583,200	39,200	0
34	8399	3,359,600	3,360,000	46,800	3,296,000	17,200	0	46,800	3,313,200	0	0
35	10,989	4,395,600	4,396,000	962,800	3,171,200	262,000	0	962,800	3,321,200	112,000	0
36	55,868	22,347,200	22,048,000	972,400	14,896,400	4,391,600	1,787,200	972,400	15,498,800	4,677,600	898,800
37	7924	3,169,600	3,170,000	59,200	3,007,600	103,200	0	59,200	3,098,800	12,000	0
38	5642	2,256,800	2,257,200	0	1,971,600	285,600	0	0	2,196,400	60,800	0
39	15,993	6,397,200	6,397,600	3200	5,160,800	1,229,600	0	3200	5,639,600	750,800	0
40	No outlet	–	17,480,440	226,800	15,170,400	1,727,600	314,800	226,800	15,460,000	1,659,200	93,600

(continued on next page)

Table 3 (continued)

ID	N# of vents	Lava volume	Perimeter on the map	Average spatial intensity	Average height of watershed boundary (ridge)			Average height of drainage system			Difference		Volume capacity	
	Within a watershed				Mean	Median	Std dev	Mean	Median	Std dev	Mean	Median		
Unit	Number	km <sup>3</sup>	m	Vent/Km <sup>2</sup>	m			m			m		m <sup>3</sup>	
1	0	0	8680	0.00	72.54	77.74	25.80	14.83	16.26	6.98	57.71	61.48	67,448,589	
2	0	0	8960	0.02	80.88	88.02	22.97	14.67	15.65	8.30	66.21	72.37	73,222,025	
3	1	(Unmeasured)	21,640	0.37	54.18	59.14	26.93	17.96	17.33	6.53	36.22	41.81	259,637,000	
4	0	0	13,560	0.88	43.87	34.55	27.44	15.24	17.83	10.17	28.63	16.72	57,590,928	
5	0	0	15,080	0.13	76.55	83.47	22.47	14.50	14.68	9.15	62.05	68.79	177,746,866	
6	0	0	8600	0.02	57.00	59.64	28.17	15.21	12.45	8.08	41.79	47.19	23,584,874	
7	1	(Unmeasured)	8280	0.87	47.66	47.71	22.77	8.27	4.67	7.80	39.39	43.04	33,073,636	
8	0	0	7880	1.26	39.40	46.92	24.22	5.07	4.08	2.77	34.33	42.84	19,609,298	
9	2	(Unmeasured)	11,120	2.01	45.98	50.17	30.05	5.50	3.73	3.76	40.48	46.44	33,245,378	
10	0	0	10,360	0.71	48.21	51.25	16.68	11.34	11.30	6.60	36.87	39.95	44,224,369	
11	2	92,625,870	21,320	1.32	55.51	49.28	34.47	25.22	24.80	12.40	30.29	24.48	94,930,518	
12	4	93,373,840	19,400	2.57	79.96	85.71	34.58	45.14	56.69	29.66	34.82	29.02	195,929,114	
13	2	(Unmeasured)	7360	1.87	46.32	47.79	23.19	9.60	6.33	7.79	36.72	41.46	16,867,823	
14	2	80,034,090	25,800	1.19	57.14	57.84	30.27	35.79	39.12	18.77	21.35	18.72	158,501,042	
15	2	25,171,120	28,680	0.83	64.50	68.04	25.09	39.95	46.47	16.56	24.55	21.57	202,682,174	
16	0	0	27,880	0.25	53.95	57.42	23.14	18.68	17.11	11.57	35.27	40.31	205,096,408	
17	1	52,020,000	14,000	1.55	76.14	81.16	36.44	38.44	54.17	25.28	37.70	26.99	51,242,497	
18	4	307,467,100	31,000	1.52	56.27	52.12	34.92	31.40	30.86	19.39	24.87	21.26	466,590,181	
19	0	0	8320	0.85	39.27	42.69	18.83	3.90	3.44	1.01	35.37	39.25	22,264,479	
20	2	(Unmeasured)	11,000	1.04	40.59	43.09	14.15	16.23	14.71	6.86	24.36	28.38	33,184,163	
21	2	9,338,770	15,440	1.29	42.31	42.91	25.07	14.69	13.94	10.02	27.62	28.97	78,930,672	
22	2	24,359,770	9520	1.53	38.72	38.64	20.65	19.91	16.65	8.13	18.81	21.99	6,209,318	
23	0	0	10,720	0.45	26.24	23.95	12.73	6.62	7.07	3.15	19.62	16.88	25,605,477	
24	1	(Unmeasured)	21,360	0.31	35.61	30.38	20.45	16.03	16.32	8.21	19.58	14.06	70,992,050	
25	1	1,921,990	10,720	1.57	24.17	22.60	12.25	7.89	8.27	1.78	16.28	14.33	14,354,005	
26	1	33,815,100	18,600	1.42	26.76	28.06	12.59	12.21	6.29	9.04	14.55	21.77	34,154,080	
27	2	(Unmeasured)	15,800	1.15	41.52	30.01	32.99	15.07	15.54	8.07	26.45	14.47	72,872,974	
28	0	0	8960	0.26	78.19	77.72	29.77	16.75	13.27	13.05	61.44	64.45	7,685,945	
29	2	(Unmeasured)	29,920	0.73	53.57	33.42	39.24	22.46	19.45	13.75	31.11	13.97	475,496,577	
30	0	0	20,000	1.15	19.44	20.21	5.74	7.53	6.97	4.16	11.91	13.24	25,563,064	
31	0	(Unmeasured)	13,560	0.95	12.67	11.97	4.78	4.75	4.80	2.53	7.92	7.17	12,510,351	
32	1	5,585,270	16,840	1.19	20.96	16.05	17.34	7.94	7.04	2.27	13.02	9.01	22,370,090	
33	3	1,205,530	14,640	1.62	16.16	16.02	4.03	5.27	5.04	2.88	10.89	10.98	24,694,262	
34	0	0	12,360	0.52	10.05	6.62	5.73	5.17	5.03	1.37	4.88	1.59	6,348,976	
35	2	(Unmeasured)	15,240	1.33	23.83	24.54	4.60	12.69	15.56	5.53	11.14	8.98	29,670,382	
36	3	8,637,990	37,840	0.69	47.28	27.37	37.76	25.06	20.91	16.19	22.22	6.46	219,321,351	
37	0	0	10,640	1.09	24.61	26.01	8.38	9.53	9.01	6.79	15.08	17.00	11,093,630	
38	0	0	9,720	0.38	25.34	28.84	8.81	12.66	13.88	7.85	12.68	14.96	6,053,654	
39	0	0	18,960	0.14	27.03	28.25	15.23	12.14	11.62	9.98	14.89	16.63	24,463,943	
40	0	0	21,242	0.00	36.12	24.38	33.22	13.78	10.02	14.99	22.34	14.36	141,708,902	
											MEAN	28.29	27.58	88,669,277
											MAX	66.21	72.37	475,496,577
											MIN	4.88	1.59	6,053,654

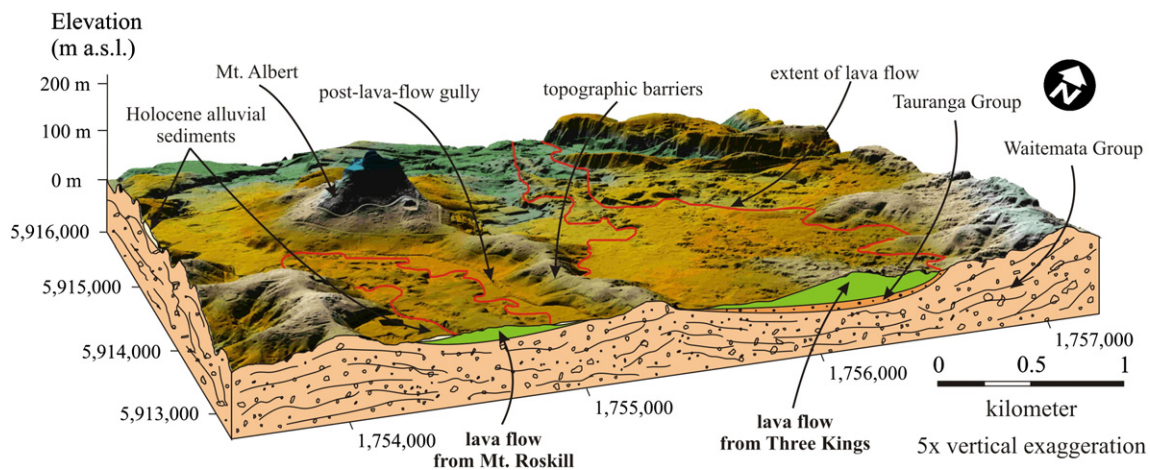
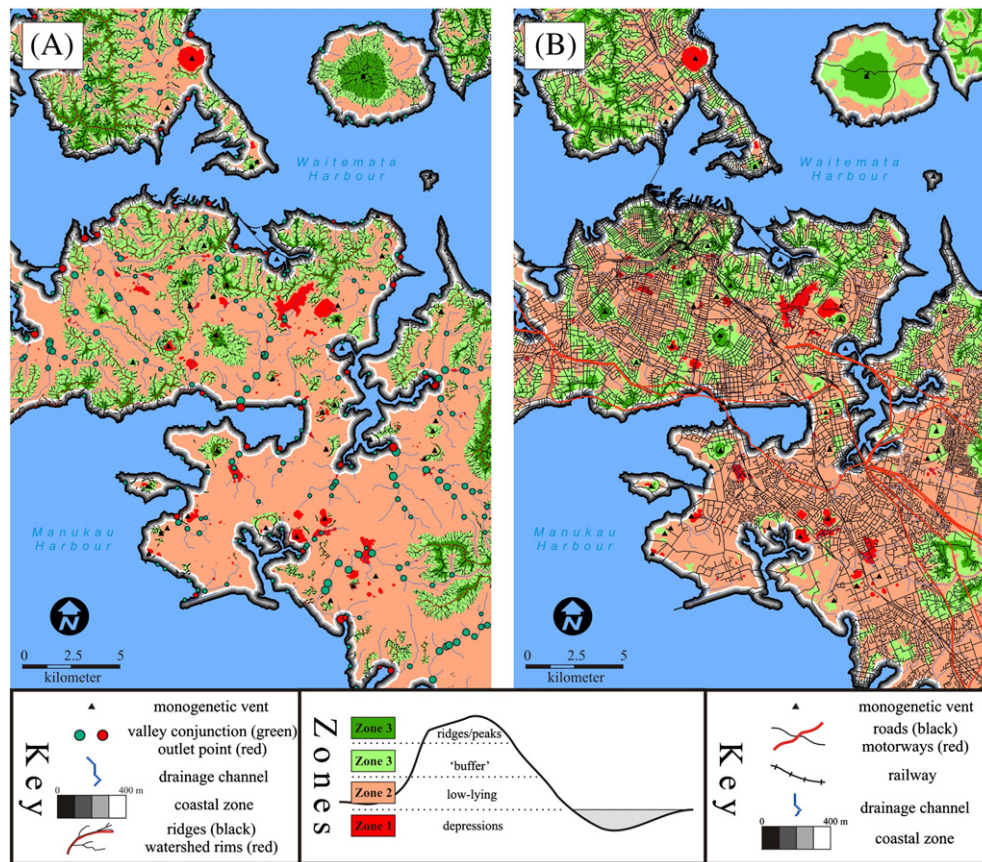


Fig. 8. Cross-section through the central, elevated part, of Auckland, illustrating the channelized lava flows by valley eroded into the Waitemata sandstone. For the detailed location see Fig. 1.



**Fig. 9.** Lava flow susceptibility map based on Scenario 1 (without Rangitoto) for the City of Auckland showing the susceptibility zones with the major hydrological and topographical characteristics (A) and with major infrastructures (B).

## 5.2. Watershed characteristics

The lava flow susceptibility map (Fig. 9) does not provide information about the location of future eruption(s), but the spatial intensity of past eruptions may give us a general picture of vent concentrations. These higher intensity regions may be the likely locations of future vents if the spatial controls, such as stress field, faulting or location of melt source in the mantle, still remain the same as they were in the past (Fig. 7). Nevertheless, not all of the vents in Auckland produced lava flows, making spatial intensity values somewhat unreliable for lava flow hazard assessment. For instance, some vents located in both the northern and southern parts, were formed by hydromagmatic eruptions and are presented by tuff rings, maars and tuff cones (Allen & Smith, 1994; Allen et al., 1996; Smith et al., 2008). A consequence of the negative, crater-like shape of such volcanic features is that any late-stage effusive activity was generally emplaced within the previously formed crater, creating lava lakes rather than flows, e.g. Crater Hill (Allen et al., 1996). Thus, they did not cover an extended area. A similar outcome is expected during a future eruption where lava effusion follows phreatomagmatic activity. The volume distribution of the lava flows examined within watersheds coincides with the spatial intensity peaks, because the centrally located watersheds hosted the majority of the large volume lava flows volumes, excluding Rangitoto (Fig. 7). The largest volume ( $0.3 \text{ km}^3$ ) hosted by a single watershed is observed in the case ID18, containing One Tree Hill (Figs. 1 and 7). This watershed (ID18) also has a large volume-capacity ( $0.46 \text{ km}^3$ ), which means that if a future eruption does not exceed this volume; the flows will be controlled by the topographical extent of this watershed.

The proportion of susceptibility zones within watersheds reveals that the geographical locations of safe zones are highly scattered and mostly

concentrated in the central and northern part of the field (Fig. 7). The difference between the scenarios (i.e. without and with Rangitoto), causes only a slight decrease in the area of buffer zone and ridges in Scenario 2. The majority of the centrally located watersheds also have a significant proportion of predominantly flat areas, which favours the spreading of a lava flow over the topography in some cases  $> 50\%$  of the watershed. Nevertheless, the elevation of the rim of each watershed is high enough ( $\geq T_{\text{mean}}$  or  $\geq 15 \text{ m}$ ) to hinder the overspill of lava flows to neighbouring watersheds. The larger watersheds, such as ID 14 or 18 in the central area, have a high proportion of depressions and low-lying areas (Fig. 7). Finally, the highest likelihood of future topographically-controlled lava flow emplacement occurs at the northern edge of the City of Auckland. In this area the total proportion of buffer and ridges zones within a watershed is generally  $> 50\%$ . In contrast, the southern parts are almost completely lacking in topographically elevated ridges or hill tops (Figs. 7 and 9).

## 5.3. Evaluation of the method and its limitations

There are a few limitations of the mapping technique presented. For instance, future eruptions may occur on a ridge, possibly feeding multiple watersheds. The possibility of an eruption on a ridge (or local topographical highs) is likely when the magma supply is high enough to generate faulting. This is possible expected in the case of high-magma-flux volcanic fields that are often magmatically-controlled (Valentine & Krogh, 2006; Valentine & Perry, 2007). The magma supply of most of the eruptive centres in Auckland was in the range of  $\leq 0.25 \text{ km}^3$ , excluding One Tree Hill and Rangitoto (Table 1). This is in the range of the typical, intraplate monogenetic eruptive volume values (e.g. Valentine & Perry, 2006). In addition, the central part of Auckland, where watershed-controlled behaviour of a future lava flow is expected, a few normal faults have been

identified (e.g. Kenny et al., 2011). The combination of the limited magma supply with the presence of large-scale faulting means, the propagation of magma related to a future eruption is expected to be captured by the pre-existing structural features. This means that vent-position of a future eruption is more likely to be situated within the valleys (or watershed) and not on the ridges if the magma supply of a future eruption remains in the same range as it was in the past eruptions. On this theoretical basis, the delimited ridges could be interpreted as the safest places during a future effusive eruption. This is in further agreement with the fact that most of the past eruptive centres are located within valleys and not on the ridges. Thus, in the localisation of the monogenetic volcanism, the topography may have played a major role.

Another limitation of the method (and all such methods) is the possibility of phreatomagmatic explosion forming craters that can control the subsequent lava flow emplacement. This scenario is especially important in the southern, low-lying area, where porous-controlled, water-saturated alluvial sediments are common (Kermode, 1992), which are able to fuel phreatomagmatic eruptions (Houghton et al., 1996). There is also possibility in future events that the topography will be altered or watersheds become truncated by various large-scale eruptive processes that will require a dynamic lava flow modelling approach and/or a continuous update of topographically delimited hazard zones.

Finally, some limitation and uncertainty in the delimited susceptibility zones may derive from the under- or overestimate of lava flow thickness preserved in the past lava flows due to accuracy of the basement reconstructed beneath the volcanic edifices and lava flows.

## 6. Conclusions

The City of Auckland is highly susceptible to lava flows, which are likely to travel further, and be potentially more destructive to infrastructure over longer periods, than the products of explosive opening phases of monogenetic eruptions at Auckland. Past lava flows in Auckland totalled  $>2 \text{ km}^3$  in volume (mostly produced during the last 40 ka), with average flows reaching 2.5 km (up to 6.5 km) and with a mean thickness of  $\sim 14.8 \text{ m}$ . They covered areas up to  $>25 \text{ km}^2$ , but on average  $5.1 \text{ km}^2$ .

Two scenarios were tested using two different lava-thickness threshold values calculated directly from the flow properties. These scenarios showed that the study area can be split into two regions, south and north: the southern part lacks large-scale topographical boundaries (ridges) that can significantly control the pathways of future lava flows, whereas in the north, ridges of underlying sandstone are prominent enough to potentially control the distribution and shape of future lava flows. The field also lacks large depressions that can be lava depocentres. Extremely long lava flows are hence only expected from future Auckland eruptions located in topographically constrained portions of the central/northern region of the field.

The range of methods applied here are available in free or commercial GIS software packages, and when combined they provide valuable results that can be used for lava flow susceptibility mapping. In addition, freely available remotely-sensed Digital Terrain Models, such as 30 m or 90 m STRM, provide opportunities giving place for increasing lava flow susceptibility modelling over monogenetic volcanic fields worldwide.

The major advantage of this method is that it is suitable for modelling lava flow susceptibility for monogenetic volcanic field, where not eye-witnessed eruption was recorded. This method is also vent-location independent because it is based on morphometric characteristics of past lava flows and the present state of the topography. The compiled lava flow susceptibility map is based on detecting relative topographic difference as compared to the local low point (bottom of drainage channels) improving the adaptive nature of this technique. This method can be used as an input map for detailed dynamic lava flow simulations. Due to the very flat morphology of the southern part of Auckland, thermorheological-dependent

models rather than topography-dependent models are more favourable for modelling lava flow pathways.

## Acknowledgements

GK would like to thank to the PhD Research Fellowship offered by the Institute of Natural Resources at Massey University (New Zealand). This work was also supported by the FRST-IIOF project “Facing the challenge of Auckland’s volcanism”. The authors would like to thank the help of Fugro Spatial Solutions and New Zealand Aerial Mapping Limited for the survey details, and to the Auckland City Council for the use of the LiDAR dataset.

## References

- Aguilar, F. J., Agüera, F., Aguilar, M. A., & Carvajal, F. (2005). Effects of terrain morphology, sampling density, and interpolation methods on grid DEM accuracy. *Photogrammetric Engineering and Remote Sensing*, 71, 805–816.
- Aguilar, F. J., & Mills, J. P. (2008). Accuracy assessment of LiDAR-derived digital elevation models. *The Photogrammetric Record*, 23, 148–169.
- Allen, S. R., Bryner, V. F., Smith, I. E. M., & Ballance, P. F. (1996). Facies analysis of pyroclastic deposits within basaltic tuff-rings of the Auckland volcanic field, New Zealand. *New Zealand Journal of Geology and Geophysics*, 39, 309–327.
- Allen, S. R., & Smith, I. E. M. (1994). Eruption styles and volcanic hazard in the Auckland Volcanic Field, New Zealand. *Geoscience Reports of Shizuoka University*, 20, 5–14.
- Ashenden, C. L., Lindsay, J. M., Sherburn, S., Smith, I. E., Miller, C. A., & Malin, P. E. (2011). Some challenges of monitoring a potentially active volcanic field in a large urban area: Auckland volcanic field, New Zealand. *Natural Hazards*, 59, 507–528.
- Barberi, F., Carapezza, M. L., Valenza, M., & Villar, L. (1993). The control of lava flow during the 1991–1992 eruption of Mt. Etna. *Journal of Volcanology and Geothermal Research*, 56, 1–34.
- Bebbington, M. S., & Cronin, S. J. (2011). Spatio-temporal hazard estimation in the Auckland Volcanic Field, New Zealand, with a new event-order model. *Bulletin of Volcanology*, 73, 55–72.
- Bonne, K., Kervyn, M., Cascone, L., Njome, S., Van Ranst, E., Suh, E., et al. (2008). A new approach to assess long-term lava flow hazard and risk using GIS and low-cost remote sensing: the case of Mount Cameroon, West Africa. *International Journal of Remote Sensing*, 29, 6539–6564.
- Briggs, R. M., & McDonough, W. F. (1990). Contemporaneous Convergent Margin and Intraplate Magmatism, North Island, New Zealand. *Journal of Petrology*, 31, 813–951.
- Briggs, R. M., Okada, T., Itaya, T., Shibuya, H., & Smith, I. E. M. (1994). K–Ar ages, paleomagnetism, and geochemistry of the South Auckland volcanic field, North Island, New Zealand. *New Zealand Journal of Geology and Geophysics*, 37, 143–153.
- Cassidy, J., & Locke, C. A. (2010). The Auckland volcanic field, New Zealand: Geophysical evidence for structural and spatio-temporal relationships. *Journal of Volcanology and Geothermal Research*, 195, 127–137.
- Connor, L. J., Connor, C. B., Meliksetian, K., & Savov, I. (2012). Probabilistic approach to modeling lava flow inundation: a lava flow hazard assessment for a nuclear facility in Armenia. *Journal of Applied Volcanology*, 1(3). [<http://www.appliedvolc.com/1/1/3/>]
- Connor, C. B., & Hill, B. E. (1995). Three nonhomogeneous Poisson models for the probability of basaltic volcanism: Application to the Yucca Mountain region, Nevada, U.S.A. *Journal of Geophysical Research*, 100, 10107–10125.
- Cook, C., Briggs, R. M., Smith, I. E. M., & Maas, R. (2005). Petrology and geochemistry of intraplate basalts in the South Auckland volcanic field, New Zealand: Evidence for two coeval magma suites from distinct sources. *Journal of Petrology*, 46, 473–503.
- Costa-Cabral, M. C., & Burges, S. J. (1994). Digital elevation model networks (DEMOM): A model of flow over hillslopes for computations of contributing and dispersal areas. *Water Resources Research*, 30, 1681–1692.
- Crisci, G. M., Rongo, R., Di Gregorio, S., & Spataro, W. (2004). The simulation model SCIARA: The 1991 and 2001 lava flows at Mount Etna. *Journal of Volcanology and Geothermal Research*, 132, 253–267.
- Del Negro, C., Fortuna, L., Herault, A., & Vicari, A. (2008). Simulations of the 2004 lava flow at Etna volcano using the magflow cellular automata model. *Bulletin of Volcanology*, 70, 805–812.
- Douglas, D. H. (1986). Experiments to locate ridges and channels to create a new type of digital elevation models. *Cartographica*, 23, 29–61.
- Dragoni, M., & Tallarico, A. (1994). The effect of crystallization on the rheology and dynamics of lava flows. *Journal of Volcanology and Geothermal Research*, 59, 241–252.
- Duong, T. (2007). ks: Kernel density estimation and kernel discriminant analysis for multivariate data in R. *Journal of Statistical Software*, 21, 1–16.
- Eade, J. (2009). Petrology and correlation of lava flows from the central part of the Auckland Volcanic Field. *Unpublished Msc thesis, University of Auckland*, 1–88.
- Edbrooke, S. W. (2001). *Geology of the Auckland area*. Scale 1:250,000. Lower Hutt, New Zealand: Institute of Geological & Nuclear Sciences.
- Edbrooke, S. W., Mazengarb, C., & Stephenson, W. (2003). Geology and geological hazards of the Auckland urban area, New Zealand. *Quaternary International*, 103, 3–21.

- Favalli, M., Fornaciari, A., Mazzarini, F., Harris, A., Neri, M., Behncke, B., et al. (2010). Evolution of an active lava flow field using a multitemporal LIDAR acquisition. *Journal of Geophysical Research*, 115.
- Favalli, M., Fornaciari, A., & Pareschi, M. T. (2009a). LIDAR strip adjustment: Application to volcanic areas. *Geomorphology*, 111, 123–135.
- Favalli, M., Mazzarini, F., Pareschi, M. T., & Boschi, E. (2009b). Topographic control on lava flow paths at Mount Etna, Italy: Implications for hazard assessment. *Journal of Geophysical Research*, 114.
- Favalli, M., Pareschi, M. T., Neri, A., & Isola, I. (2005). Forecasting lava flow paths by a stochastic approach. *Geophysical Research Letters*, 32.
- Favalli, M., Tarquini, S., Fornaciari, A., & Boschi, E. (2009c). A new approach to risk assessment of lava flow at Mount Etna. *Geology*, 37, 1111–1114.
- Felpeito, A., Araña, V., Ortiz, R., Astiz, M., & García, A. (2001). Assessment and modelling of lava flow hazard on Lanzarote (Canary Islands). *Natural Hazards*, 23, 247–257.
- Ganci, G., Vicari, A., Cappello, A., & Del Negro, C. (2012). An emergent strategy for volcano hazard assessment: From thermal satellite monitoring to lava flow modeling. *Remote Sensing of Environment*, 119, 197–207.
- Garbrecht, J., & Martz, L. W. (1995). TOPAZ: An automated digital landscape analysis tool for topographic evaluation, drainage identification, watershed segmentation and subcatchment parameterisation: TOPAZ User Manual. El Reno, Oklahoma: U.S. Department of Agriculture.
- Garbrecht, J., & Martz, L. W. (1997). The assignment of drainage direction over flat surfaces in raster digital elevation models. *Journal of Hydrology*, 193, 204–213.
- Griffiths, R. W. (2000). The dynamics of lava flows. *Annual Review of Fluid Mechanics*, 32, 477–518.
- Harris, A. J. L., & Baloga, S. M. (2009). Lava discharge rates from satellite-measured heat flux. *Geophysical Research Letters*, 36. <http://dx.doi.org/10.1029/2009GL039717>.
- Harris, A. J., Dehn, J., & Calvari, S. (2007). Lava effusion rate definition and measurement: A review. *Bulletin of Volcanology*, 70, 1–22.
- Harris, A. J. L., Favalli, M., Steffke, A., Fornaciari, A., & Boschi, E. (2010). A relation between lava discharge rate, thermal insulation, and flow area set using lidar data. *Geophysical Research Letters*, 37. <http://dx.doi.org/10.1029/2010GL044683>.
- Harris, A. J. L., Flynn, L. P., Keszthelyi, L., Mougini-Mark, P. J., Rowland, S. K., & Resing, J. A. (1998). Calculation of lava effusion rates from Landsat TM data. *Bulletin of Volcanology*, 60, 52–71.
- Harris, A. J. L., & Rowland, S. K. (2001). FLOWGO: A kinematic thermorheological model for lava flowing in a channel. *Bulletin of Volcanology*, 63, 20–44.
- Hayward, B. W., Murdoch, G., & Maitland, G. (2011). *Volcanoes of Auckland*. Auckland, New Zealand: Auckland University Press.
- Herauld, A., Vicari, A., Ciraud, A., & Del Negro, C. (2009). Forecasting lava flow hazard during the 2006 Etna eruption: Using the Magflow cellular automata model. *Computers & Geosciences*, 35, 1050–1060.
- Hidaka, M., Goto, A., Susumu, U., & Fujita, E. (2005). VTFS project: Development of the lava flow simulation code LavaSIM with a model for three-dimensional convection, spreading, and solidification. *Geochemistry, Geophysics, Geosystems*, 6. <http://dx.doi.org/10.1029/2004GC000869>.
- Hirano, A., Welch, R., & Lang, H. (2003). Mapping from ASTER stereo image data: DEM validation and accuracy assessment. *ISPRS Journal of Photogrammetry and Remote Sensing*, 57, 356–370.
- Hodder, A. P. W. (1984). Late Cenozoic rift development and intra-plate volcanism in northern New Zealand inferred from geochemical discrimination diagrams. *Tectonophysics*, 101, 293–318.
- Houghton, B. F., Wilson, C. J. N., Rosenberg, M. D., Smith, I. E. M., & Parker, R. J. (1996). Mixed deposits of complex magmatic and phreatomagmatic volcanism: An example from Crater Hill, Auckland, New Zealand. *Bulletin of Volcanology*, 58, 59–66.
- Houghton, B. F., Wilson, C. J. N., & Smith, I. E. M. (1999). Shallow-seated controls on styles of explosive basaltic volcanism: a case study from New Zealand. *Journal of Volcanology and Geothermal Research*, 91, 97–120.
- Jenson, S. K., & Domingue, J. O. (1988). Extracting topographic structure from digital elevation data for geographic information system analysis. *Photogrammetric Engineering and Remote Sensing*, 54, 1593–1600.
- Jones, K. H. (1998). A comparison of algorithms used to compute hill slope as a property of the DEM. *Computers & Geosciences*, 24, 315–323.
- Jordan, G. (2003). Morphometric analysis and tectonic interpretation of digital terrain data: A case study. *Earth Surface Processes and Landforms*, 28, 807–822.
- Jordan, G. (2007a). Adaptive smoothing of valleys in DEMs using TIN interpolation from ridge line elevations: An application to morphotectonic aspect analysis. *Computers & Geosciences*, 33, 573–585.
- Jordan, G. (2007b). Digital terrain analysis in a GIS environment. Concepts and development. In R. J. Peckham, & G. Jordan (Eds.), *Digital terrain modelling. Development and applications in a policy support environment* (pp. 1–43). Berlin: Springer.
- Jordan, G., & Schott, B. (2005). Application of wavelet analysis to the study of spatial pattern of morphotectonic lineaments in digital terrain models. A case study. *Remote Sensing of Environment*, 93, 31–38.
- Jurado-Chichay, Z., Rowland, S. K., & Walker, G. P. L. (1996). The formation of circular littoral cone from tube-fed pahoehoe: Mauna Loa, Hawaii. *Bulletin of Volcanology*, 57, 471–482.
- Kenny, J. A., Lindsay, J., & Howe, T. M. (2011). Large-scale faulting in the Auckland Region. *IESE Report 1–2011.04* (pp. 1–98).
- Kereszturi, G., & Németh, K. (2012). Structural and morphometric irregularities of eroded Pliocene scoria cones at the Bakony–Balaton Highland Volcanic Field, Hungary. *Geomorphology*, 136, 45–58.
- Kereszturi, G., Németh, K., Csillag, G., Balogh, K., & Kovács, J. (2011). The role of external environmental factors in changing eruption styles of monogenetic volcanoes in a Mio/Pleistocene continental volcanic field in western Hungary. *Journal of Volcanology and Geothermal Research*, 201, 227–240.
- Kermode, L. (1992). *Geology of the Auckland urban area*. Scale 1:50,000. Lower Hutt, New Zealand: Institute of Geological and Nuclear Sciences.
- Kervyn, M., Ernst, G. G. J., Goossens, R., & Jacobs, P. (2008). Mapping volcano topography with remote sensing: ASTER vs. SRTM. *International Journal of Remote Sensing*, 29, 6515–6538.
- Lindsay, J. M., Leonard, G. S., Smid, E. R., & Hayward, B. W. (2011). Age of the Auckland Volcanic Field: A review of existing data. *New Zealand Journal of Geology and Geophysics*, 54, 379–401.
- Lindsay, J., Marzocchi, W., Jolly, G., Constantinescu, R., Selva, J., & Sandri, L. (2010). Towards real-time eruption forecasting in the Auckland Volcanic Field: Application of BET\_EF during the New Zealand National Disaster Exercise 'Ruaumoko'. *Bulletin of Volcanology*, 72, 185–204.
- Lombardo, V., & Buongiorno, M. F. (2006). Lava flow thermal analysis using three infrared bands of remote-sensing imagery: A study case from Mount Etna 2001 eruption. *Remote Sensing of Environment*, 101, 141–149.
- Magill, C., & Blong, R. (2005a). Volcanic risk ranking for Auckland, New Zealand. I: Methodology and hazard investigation. *Bulletin of Volcanology*, 67, 331–339.
- Magill, C., & Blong, R. (2005b). Volcanic risk ranking for Auckland, New Zealand. II: Hazard consequences and risk calculation. *Bulletin of Volcanology*, 67, 340–349.
- Magill, C., Blong, R., & McAneney, J. (2005). VolcanZ—A volcanic loss model for Auckland, New Zealand. *Journal of Volcanology and Geothermal Research*, 149, 329–345.
- Mark, D. M. (1984). Automatic detection of drainage networks from digital elevation models. *Cartographica*, 21, 168–178.
- Marti, J., Planagumà, L., Geyer, A., Canal, E., & Pedrazzi, D. (2011). Complex interaction between Strombolian and phreatomagmatic eruptions in the Quaternary monogenetic volcanism of the Catalan Volcanic Zone (NE of Spain). *Journal of Volcanology and Geothermal Research*, 201, 178–193.
- Martz, L. W., & Garbrecht, J. (1992). Numerical definition of drainage networks and subcatchment areas from digital elevation models. *Computers and Geosciences*, 18, 747–761.
- Martz, L. W., & Garbrecht, J. (1999). An outlet breaching algorithm for the treatment of closed depressions in a raster DEM. *Computers & Geosciences*, 25, 835–844.
- Mattox, T. N., & Mangan, M. T. (1997). Littoral hydrovolcanic explosions: A case study of lava–seawater interaction at Kilauea volcano. *Journal of Volcanology and Geothermal Research*, 75, 1–17.
- Mazzarini, F., Pareschi, M. T., Favalli, M., Isola, I., Tarquini, S., & Boschi, E. (2005). Morphology of basaltic lava channels during the Mt. Etna September 2004 eruption from airborne laser altimeter data. *Geophysical Research Letters*, 32.
- McGee, L. E., Beier, C., Smith, I. E. M., & Turner, S. P. (2011). Dynamics of melting beneath a small-scale basaltic system: A U–Th–Ra study from Rangitoto volcano, Auckland volcanic field, New Zealand. *Contributions to Mineralogy and Petrology*, 162, 547–563.
- Molloy, C., Shane, P., & Augustinus, P. (2009). Eruption recurrence rates in a basaltic volcanic field based on tephra layers in maar sediments: Implications for hazards in the Auckland volcanic field. *Geological Society of America Bulletin*, 121, 1666–1677.
- Moore, I. D., Grayson, R. B., & Landson, A. R. (1991). Digital terrain modelling: A review of hydrological, geomorphological, and biological applications. *Hydrological Processes*, 5, 3–30.
- Morris, D. G., & Heerdegen, R. G. (1988). Automatically derived catchment boundary and channel networks and their hydrological applications. *Geomorphology*, 1, 131–141.
- Mougini-Mark, P. J., & Garbeil, H. (2005). Quality of TOPSAR topographic data for volcanology studies at Kilauea Volcano, Hawaii: An assessment using airborne lidar data. *Remote Sensing of Environment*, 96, 149–164.
- Needham, A. J., Lindsay, J. M., Smith, I. E. M., Augustinus, P., & Shane, P. A. (2011). Sequential eruption of alkaline and sub-alkaline magmas from a small Monogenetic volcano in The Auckland Volcanic Field, New Zealand. *Journal of Volcanology and Geothermal Research*, 201, 126–142.
- Németh, K., Goth, K., Martin, U., Csillag, G., & Suhr, P. (2008). Reconstructing paleoenvironment, eruption mechanism and paleomorphology of the Pliocene Pula maar, (Hungary). *Journal of Volcanology and Geothermal Research*, 177, 441–456.
- Pieri, D., & Abrams, M. (2005). ASTER observations of thermal anomalies preceding the April 2003 eruption of Chikurachki volcano, Kurile Islands, Russia. *Remote Sensing of Environment*, 99, 84–94.
- Pollyea, R. M., & Fairley, J. P. (2012). Experimental evaluation of terrestrial LiDAR-based surface roughness estimates. *Geosphere*, 8, 1–7.
- Rodríguez-González, A., Fernández-Turiel, J. L., Pérez-Torrado, F. J., Aulinas, M., Carracedo, J. C., Gimeno, D., et al. (2011). GIS methods applied to the degradation of monogenetic volcanic fields: A case study of the Holocene volcanism of Gran Canaria (Canary Islands, Spain). *Geomorphology*, 134, 249–259.
- Samsonov, S., Tiampo, K., González, P. J., Manville, V., & Jolly, G. (2010). Ground deformation occurring in the city of Auckland, New Zealand, and observed by Envisat interferometric synthetic aperture radar during 2003–2007. *Journal of Geophysical Research*, 115. <http://dx.doi.org/10.1029/2009JB006806>.
- Scifoni, S., Coltelli, M., Marsella, M., Proietti, C., Napoleoni, Q., Vicari, A., et al. (2010). Mitigation of lava flow invasion hazard through optimized barrier configuration aided by numerical simulation: The case of the 2001 Etna eruption. *Journal of Volcanology and Geothermal Research*, 192, 16–26.
- Self, S., Keszthelyi, L., & Thordarson, T. (1998). The importance of pahoehoe. *Annual Review of Earth and Planetary Sciences*, 26, 81–110.
- Sharpnack, D. A., & Akin, G. (1969). An algorithm for computing slope and aspect from elevation. *Photogrammetric Survey*, 35, 247–248.
- Smith, I. E. M., & Allen, S. R. (1993). *Volcanic hazards at the Auckland volcanic field*. New Zealand: Ministry of Civil Defence.

- Smith, I. E. M., Blake, S., Wilson, C. J. N., & Houghton, B. F. (2008). Deep-seated fractionation during the rise of a small-volume basalt magma batch: Crater Hill, Auckland, New Zealand. *Contributions to Mineralogy and Petrology*, 155, 511–527.
- Spörl, K. B., & Eastwood, V. R. (1997). Elliptical boundary of an intraplate volcanic field, Auckland, New Zealand. *Journal of Volcanology and Geothermal Research*, 79, 169–179.
- Stasiuk, M. V., & Jaupart, C. (1997). Lava flow shapes and dimensions as reflections of magma system conditions. *Journal of Volcanology and Geothermal Research*, 78, 31–50.
- Su, J., & Bork, E. (2006). Influence of vegetation, slope, and lidar sampling angle on DEM accuracy. *Photogrammetric Engineering and Remote Sensing*, 72, 1265–1274.
- Székely, B., & Karátson, D. (2004). DEM-based morphometry as a tool for reconstructing primary volcanic landforms: Examples from the Börzsöny Mountains, Hungary. *Geomorphology*, 63, 25–37.
- Tarquini, S., & Favalli, M. (2011). Mapping and DOWNFLOW simulation of recent lava flow fields at Mount Etna. *Journal of Volcanology and Geothermal Research*, 204, 27–39.
- Tucker, D. S., & Scott, K. M. (2009). Structures and facies associated with the flow of subaerial basaltic lava into a deep freshwater lake: The Sulphur Creek lava flow, North Cascades, Washington. *Journal of Volcanology and Geothermal Research*, 185, 311–322.
- Valentine, G. A., & Krogh, K. E. C. (2006). Emplacement of shallow dikes and sills beneath a small basaltic volcanic center—The role of pre-existing structure (Paiute Ridge, southern Nevada, USA). *Earth and Planetary Science Letters*, 246, 217–230.
- Valentine, G. A., & Perry, F. V. (2006). Decreasing magmatic footprints of individual volcanoes in a waning basaltic field. *Geophysical Research Letters*, 33. <http://dx.doi.org/10.1029/2006GL026743>.
- Valentine, G. A., & Perry, F. V. (2007). Tectonically controlled, time-predictable basaltic volcanism from a lithospheric mantle source (central Basin and Range Province, USA). *Earth and Planetary Science Letters*, 261, 201–216.
- Vicari, A., Herault, A., Del Negro, C., Coltelli, M., Marsella, M., & Proietti, C. (2007). Simulations of the 2001 lava flow at Etna volcano by the Magflow Cellular Automata model. *Environmental Modelling and Software*, 22, 1465–1471.
- Von Veh, M. W., & Nemeth, K. (2009). An assessment of the alignments of vents on geostatistical analysis in the Auckland Volcanic Field, New Zealand. *Géomorphologie : Relief, Processus, Environnement*, 2009, 175–186.
- Walker, G. P. L. (1973). Lengths of lava flows. *Philosophical transactions of the Royal Society of London. Series A: Mathematical and Physical Sciences*, 274, 107–118.
- Wantim, M. N., Suh, C. E., Ernst, G. G. J., Kervyn, M., & Jacobs, P. (2011). Characteristics of the 2000 fissure eruption and lava flow fields at Mount Cameroon volcano, West Africa: A combined field mapping and remote sensing approach. *Geological Journal*, 46, 344–363.
- Wright, R., Flynn, L. P., Garbeil, H., Harris, A. J. L., & Pilger, E. (2004). MODVOLC: Near-real time thermal monitoring of global volcanism. *Journal of Volcanology and Geothermal Research*, 135, 29–49.